Supramolecular Chemistry
Publication details, including instructions for authors and subscription information:
http://www.informaworld.com/smpp/title~content=t713649759

Natural and Synthetic Receptors for Nitrate Anion

Oluyomi A. Okunola[a]; Paul V. Santacroce[a]; Jeffery T. Davis[a]
[a] Department of Chemistry and Biochemistry, University of Maryland, College Park, MD, USA

To cite this Article Okunola, Oluyomi A. , Santacroce, Paul V. and Davis, Jeffery T.(2008) 'Natural and Synthetic Receptors for Nitrate Anion', Supramolecular Chemistry, 20: 1, 169 — 190
To link to this Article: DOI: 10.1080/10610270701747610
URL: http://dx.doi.org/10.1080/10610270701747610

Supramolecular Chemistry, January–March 2008 Vol. 20 (1–2), pp. 169–190

Taylor & Francis
Taylor & Francis Group

Natural and Synthetic Receptors for Nitrate Anion

OLUYOMI A. OKUNOLA, PAUL V. SANTACROCE and JEFFERY T. DAVIS*

Department of Chemistry and Biochemistry, University of Maryland, College Park, MD 20742, USA

(Received 20 September 2007; Accepted 14 October 2007)

Synthetic receptors have been developed for anions such as chloride, phosphate, sulphate and carboxylate. Development of selective receptors for nitrate has, however, been more difficult. Theoretical calculations show that a six-coordinate geometry is the ideal geometry for coordinating NO_3^-. Crystallographic data show, however, that NO_3^- usually adopts a two- or three-coordinate geometry when interacting with receptors. In this review, we briefly discuss the role of NO_3^- in human health and its physical properties. We discuss how proteins and synthetic compounds bind NO_3^-, with an emphasis on crystal structures and calculations. Synthetic compounds that best mimic proteins in their types of non-covalent interactions are generally the most effective for binding NO_3^-.

Keywords: Anion recognition; Anion transport; Nitrate; Synthetic receptors

INTRODUCTION

Given the biological, environmental and chemical importance of anions, receptors for anion recognition, sensing and transport are important [1,2]. Anion complexation has its challenges. Compared with isoelectronic cations, anions are larger and have lower charge-to-size ratios. Anions come in various shapes, including spherical, linear, trigonal, tetrahedral and octahedral geometries. Anions often show multiple coordination geometries [3]. Receptors that use hydrogen bonding, hydrophobic, electrostatic and anion–π interactions are being developed for anion coordination [1–6].

We focus on nitrate (NO_3^-), an anion that has not been targeted as much as other oxyanions and halides. We briefly discuss the role of NO_3^- in human health and its physical properties. We discuss how proteins and synthetic compounds bind and transport NO_3^-, with an emphasis on crystal structures and calculations.

Nitrate and Human Health

Although nitrate is probably benign, it can be reduced to nitrite (NO_2^-), which is converted to nitric oxides [(NO_x; 7–9)]. NO_x species react with thiols, amines and amides to form carcinogenic *N*-nitroso compounds [(NOC; Scheme 1; 7–9)]. Nitric oxide (NO) and NO_2^- also react with haemoglobin to form methaemoglobin (Scheme 1). Methaemoglobin impairs blood's oxygen-carrying capacity and causes methaemoglobinaemia [8]. Other health concerns associated with NO_3^- metabolism include diabetes, thyroid disorders, respiratory infections and congenital malformations [7–9]. NO_x formation may sometimes be beneficial [7]. Potential health benefits from endogenous NO_3^-/NO_2^- including: (1) gastric protection, (2) oral/dental protection, (3) blood pressure regulation and (4) prevention of urinary tract infections.

Physical Properties of Nitrate

NO_3^- has D_{3h} symmetry with equivalent N—O bonds [(10,11; Scheme 2)]. Velders and Feil conducted a survey of NO_3^- in the cambridge structural database [(CSD; 12)]. From 338 structures, the average N—O bond length was 1.231 ± 0.025 Å and mean ONO angle was 119.98 ± 2.15°. The N—O bond lengthened as NO_3^- interacted with Lewis acids or H-bond donors. Hase reported the average bond order for nitrate as 1.278 [13]. This value varies, however, depending on the method used to determine the bond order [14]. Charge density on individual atoms also varies depending on the environment and the method used to calculate the charge density [15].

*Corresponding author. E-mail: jdavis@umd.edu

ISSN 1061-0278 print/ISSN 1029-0478 online © 2008 Taylor & Francis
DOI: 10.1080/10610270701747610

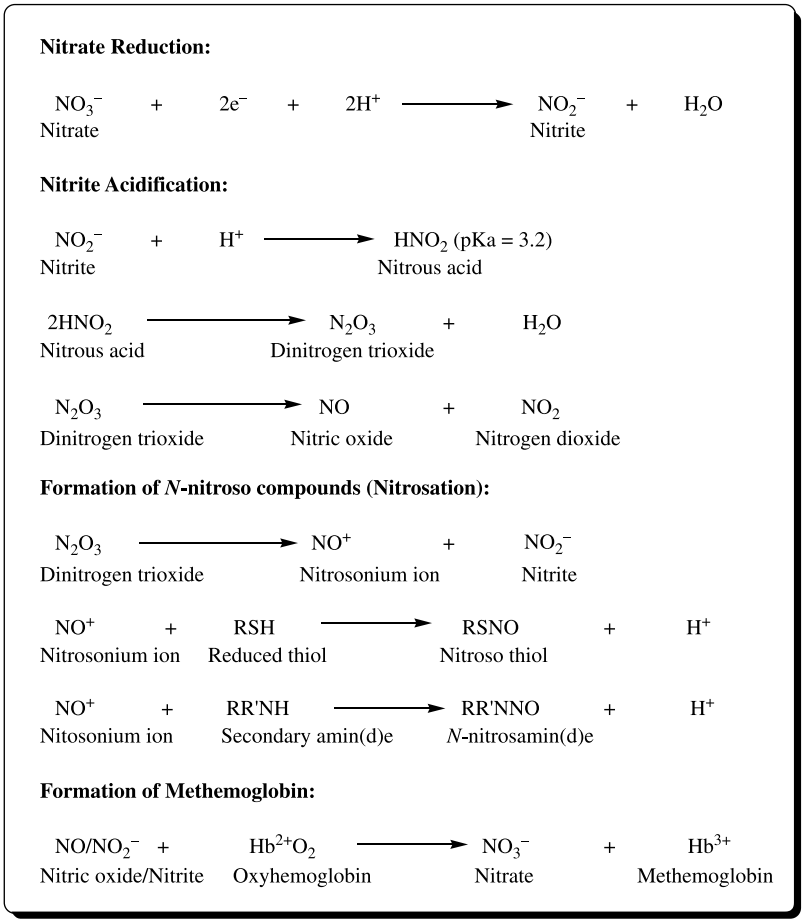

SCHEME 1 Nitrate metabolism gives reactive NO_x intermediates [(Refs.; 7–9)].

Nitrate is the conjugate base of nitric acid [($pK_a \approx -1.3$; 16)]. Nitric acid can oxidise copper and silver, whereas metals are not oxidised by HCl ($pK_a \approx -8.0$). Nitric acid is mostly dissociated in water to give NO_3^- and hydronium ions. Nitrate ions form water-soluble salts with most cations. There is an extensive hydration shell around NO_3^- [17]. Because of its heavy solvation and weak basicity, NO_3^- is weakly coordinative and it is difficult to form robust hydrogen bonds with ligands [1–6,18]. Developing NO_3^--selective receptors that use hydrogen bonds is a challenge. Synthetic receptors that use amines [19], amides [20], pyrroles [21,22], ureas [23–25] and guanidinium cations [18] have been tested for NO_3^- binding. In addition to traditional hydrogen bond donors, receptors employing aryl C—H groups and anion–π interactions have been described [26–29]. The unifying trait among these receptors is that they usually show little selectivity for NO_3^-.

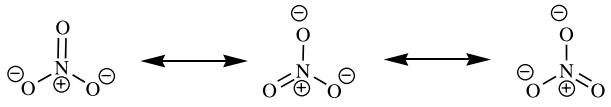

SCHEME 2 Equivalent distribution of charges on nitrate's oxygen atoms.

Theoretical Binding Motifs for Nitrate

Arranging hydrogen bond donors (D—H) on organic scaffolds is one method to make anion receptors [18–25]. Success is due to the directionality of hydrogen bonds. One can exploit directionality by designing receptors with cavities that differentiate between anions with different shapes [30,31]. Certain features are necessary for optimal hydrogen bonds between donors and acceptor atom [31–33]. These include: (1) an optimal distance, d, between donor, D—H and acceptor that gives the strongest H···O interaction; (2) a linear D—H···O bond, with D—H dipole pointing at the acceptor and (3) optimal arrangement of donors around nitrate oxygens [30–32]. The optimal distance, d, depends on the type of hydrogen bond donor, the oxyanion, anion coordination and solvent [30,31].

In a survey of NO_3^- complexes, Hay reached conclusions concerning design of NO_3^--selective receptors [30,31,34]. Hydrogen bonds were classified as follows: strong, $1.2 \leq d \geq 1.5$ Å; moderate,

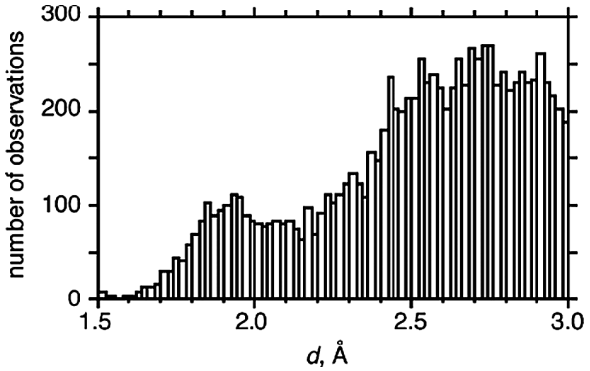

FIGURE 1 Distribution of H···O distances found in the CSD for H atoms within 3 Å of a NO_3^- oxygen atom. [Reprinted with permission from [30] Copyright © 2004 American Chemical Society].

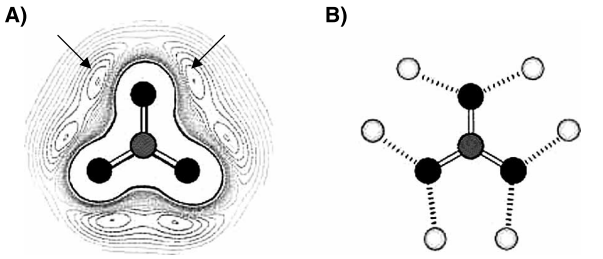

FIGURE 3 (A) Contour map of the electrostatic potential surface of NO_3^- showing the location of the six energy minima (arrows) around NO_3^-. The minima also correspond to the location of the oxygen atom lone pairs. (B) Potential binding motif for the formation of six hydrogen bonds with NO_3^-. O, black; N, dark grey; H, light grey. [Reprinted with permission from [30] Copyright © 2004 American Chemical Society].

$1.5 \leq d \geq 2.2$ Å; and weak, $2.2 \leq d \geq 3.2$ Å. A bimodal distribution of H···O distances was observed, with maxima at 1.9 and 2.7 Å (Fig. 1). Most hydrogen bonds were weak, with $d \geq 2.2$ Å. For moderate strength bonds ($d < 2.2$ Å), most contacts involved donors (D—H), where D═O or N (Fig. 2(A)), whereas above 2.3 Å (weak hydrogen bonds) most contacts were with C—H donors [30].

Hay provided evidence for hydrogen bond directionality [30,31]. Calculations revealed donor hydrogens point towards oxygens of NO_3^- with a near-linear D—H···O angle (Fig. 2(B)). Also, oxygen acceptors prefer donor hydrogens lie in the plane

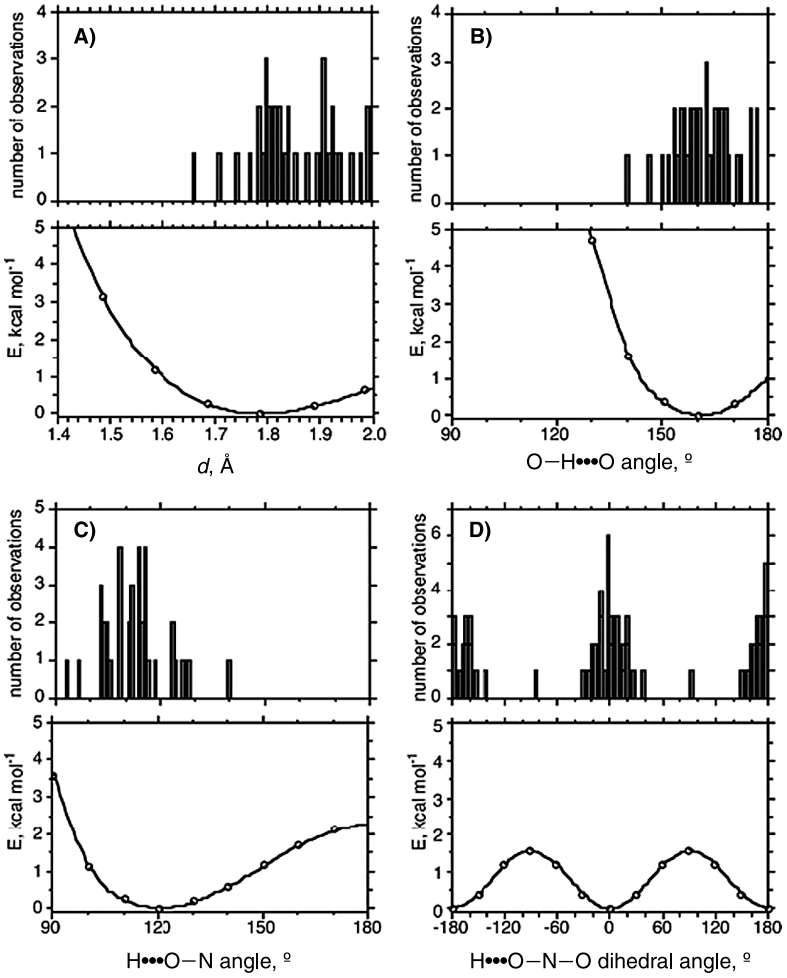

FIGURE 2 Comparison of experimental distributions of geometric parameters with potential energy surface calculations, using a MeOH—NO_3^- complex as an example: (A) optimal contact distance, *d*, (B) linear O—H···O angle, (C) bent H···O—N angle and (D) planar H···O—N—O dihedral angle. [Reprinted with permission from [30] Copyright © 2004 American Chemical Society].

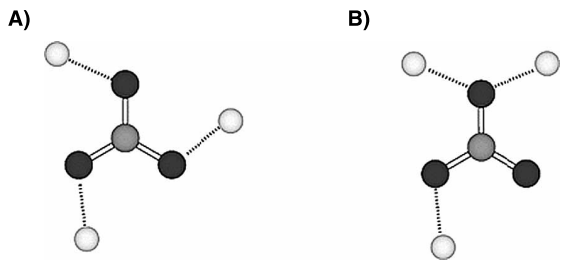

FIGURE 4 (A) The symmetric binding motif for placing three H atoms about NO_3^- using all three oxygen atoms. (B) The asymmetric motif using only two oxygen atoms with one of the oxygen atoms involved in a bifurcated hydrogen bond to two H atoms. [Reprinted with permission from [30] Copyright © 2004 American Chemical Society].

to form bent H···O—N angle (~120°; Fig. 2(C)). Finally, a planar H···O—N—O dihedral angle at 0° and/or 180° is preferred [(Fig. 2(D); 30,31)]. Electrostatic potential surfaces showed energy minima for the placement of hydrogen bonds in six equivalent positions around NO_3^-. This motif corresponded to expected locations of oxygen's lone pairs of electrons (Fig. 3). The inference is that an ideal NO_3^- receptor should have six donor D—H groups that converge at the anion's binding site (Fig. 3) [30]. In this motif, two protons share an edge of a triangle defined by NO_3^- oxygens (Fig. 3(B)). Hay's analysis of the CSD revealed, however, that only half of the six binding sites are occupied and these enable two binding modes; one motif where each of the three oxygen atoms are coordinated to one H ((Fig. 4(A)) and another where two nitrate oxygens coordinate to three H atoms (Fig. 4(B)) [30]. Examination of the CSD showed that both motifs were common in solid-state structures (Fig. 5) [30,35–40]. The explanation for use of only three out of the six possible sites is due to sterics. In a fully hydrogen-bonded complex, two protons bound to adjacent oxygens would be just ~1.86 Å apart. Such close contact would cause repulsive Coulombic and van der Waals interactions [30,41], calculated to be 16.8 kcal/mol [30].

Although C—H donors interact weakly with NO_3^-, these contacts help stabilise anion–receptor complexes [27,28]. Nitrate forms two hydrogen bond motifs with aryl C—H. Nitrate can coordinate to one C—H with two oxygens or two oxygens can bind to adjacent C—H groups (Fig. 6). Hay compared the binding energies of NO_3^-–water and NO_3^-–benzene complexes. The $NO_3^-\cdots$H—Ar interaction is indeed significant, as ΔE for $NO_3^-\cdots$H—Ar motifs were −7.50 and −9.26 kcal/mol compared with −16.03 kcal/mol for the $NO_3^-\cdots$H—OH motif (Fig. 6).

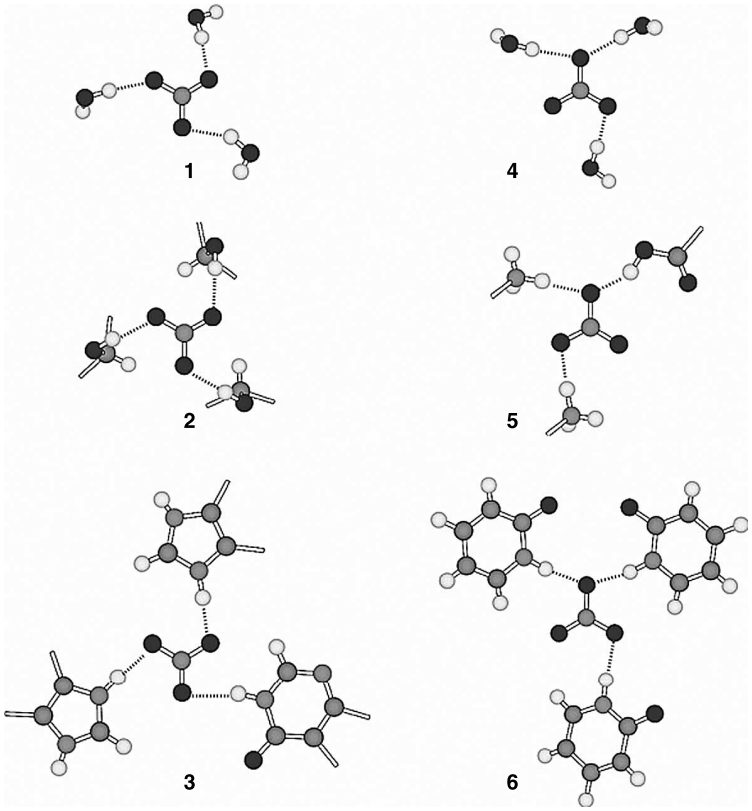

FIGURE 5 Experimental examples of hydrogen bonding motifs (Figure 4(A),(B)) found in the CSD. Only partial structures are shown for clarity. The symmetric three-oxygen motif is found in **1** [35], **2** [36] and **3** [37]. An asymmetric two-oxygen motif is found in **4** [38], **5** [39] and **6** [40]. O and H are the same as defined in figure legend **3** N/C, dark grey. [Reprinted with permission from [30] Copyright © 2004 American Chemical Society].

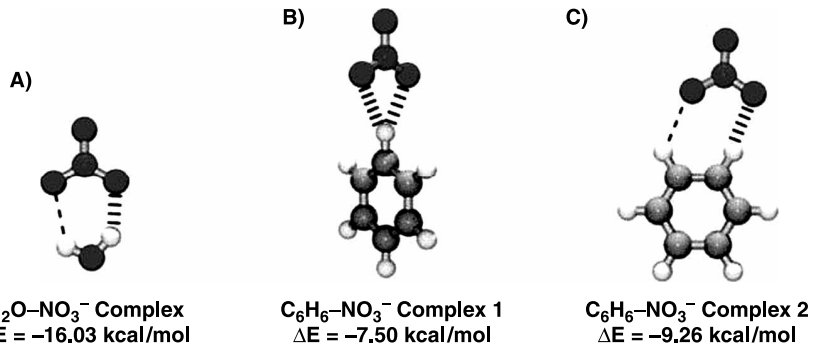

FIGURE 6 Structures and ΔE values obtained after geometry optimisation for NO_3^- complexes with (A) water and (B) and (C) benzene. The binding motif of NO_3^- with ArC—H groups where two of its oxygen atoms are coordinated to one C—H is represented in (B); (C) represents the binding motif where two oxygen atoms bind to adjacent ArC—H groups. [Reprinted with permission from [28] Copyright © 2005 American Chemical Society].

Hay's recommendation for overcoming crowding in nitrate receptors is to incorporate diprotic donors into the scaffold. Urea and guanidinium can contact two adjacent binding sites on the anion [30,42]. He recommended that acidic/aromatic C—H donors be considered as additional binding sites within a receptor [27,28].

NITRATE BINDING AND TRANSPORTING PROTEINS

Nitrate Assimilation and Uptake

Nitrogen is needed for the production of nucleic acids and proteins. Since N_2 is relatively unreactive, plants and animals obtain nitrogen from NO_3^- [43]. For humans, the major exogenous source of NO_3^- is dietary, with 80% coming from vegetables [7]. The major endogenous NO_3^- source is the L-arginine–NO pathway, where NO is synthesised from L-arginine and molecular oxygen by NO synthases (NOs;) [44]. NO reacts with oxidised haemoglobin to form NO_3^- (Scheme 1) [7,9,45]. Since, NO_3^- is a major source of nitrogen, it is important to understand how proteins assimilate NO_3^-. Studying, these proteins may help with the design of synthetic NO_3^- receptors.

Plants have three major mechanisms for transporting NO_3^- across membranes [46–48]. These are classified as follows: passive diffusion, gradient controlled and active transport. The first step in nitrate assimilation is the active transport of NO_3^- into the cell by nitrate transporter (NRT) proteins [49]. The next step is reduction of NO_3^- to NO_2^- catalysed by nitrate reductase (NR) [43,49].

Nitrate Transporter Proteins

The pK_a of HNO_3 is -1.3 [16,48]. Therefore, nitrate requires a transporter since it is deprotonated under physiological conditions and would not diffuse across a membrane [48]. Two families of NRT proteins mediate the active transport of NO_3^- across membranes: nitrate/nitrite porters (NNP) and nitrate/nitrite uptake transporters [(NitT; 50)]. The uptake of NO_3^- by NNP is proton dependent and is a H^+/NO_3^- symport process [48,50–52]. Symport involves the movement of a proton in the same direction as the anion. Other transporters move NO_3^- across membranes via an 'antiport' mechanism [46,53]. NitT proteins, also known as ABC-type NRT, mediate NO_3^- uptake by an ATP hydrolysis mechanism [48–50]. ABC-type NRT activity is inhibited by a post-translational mechanism when ammonium concentration increases to a certain level [49,54]. The NitT protein is found predominantly in bacteria. These bacteria, living in NO_3^--poor environments, probably developed ATP-driven mechanisms for survival [49,54].

The NNP Family

The proposed secondary structure of NNP proteins consists of 12 α-helical and hydrophobic transmembrane domains [55] connected by hydrophilic loops (Fig. 7). Sixteen residues are conserved among the NNP family: 2 arginines, 10 glycines, 2 phenylalanines, a tyrosine and an aspartic acid [48,52]. The two Arg residues (R87 and R368), located in helices 2 and 8, are conserved among NNP homologues (Fig. 7) and are vital for substrate binding [55,56]. The Asp residue, located on the cytoplasmic side of helix 8, is predicted to regulate NO_3^- movement by blocking anion binding by Arg 368 [48,56]. There is no crystal structure for any NNP protein. Information about the role played by individual residues has been obtained through kinetic studies of mutant proteins [55–57].

The ABC-type NRT Family

NrtABCD is composed of four polypeptide segments (Fig. 8): a periplasmic solute binder (NrtA), an integral membrane permease (NrtB), an ATPase/solute binder (NrtC) that regulates transport [58] and

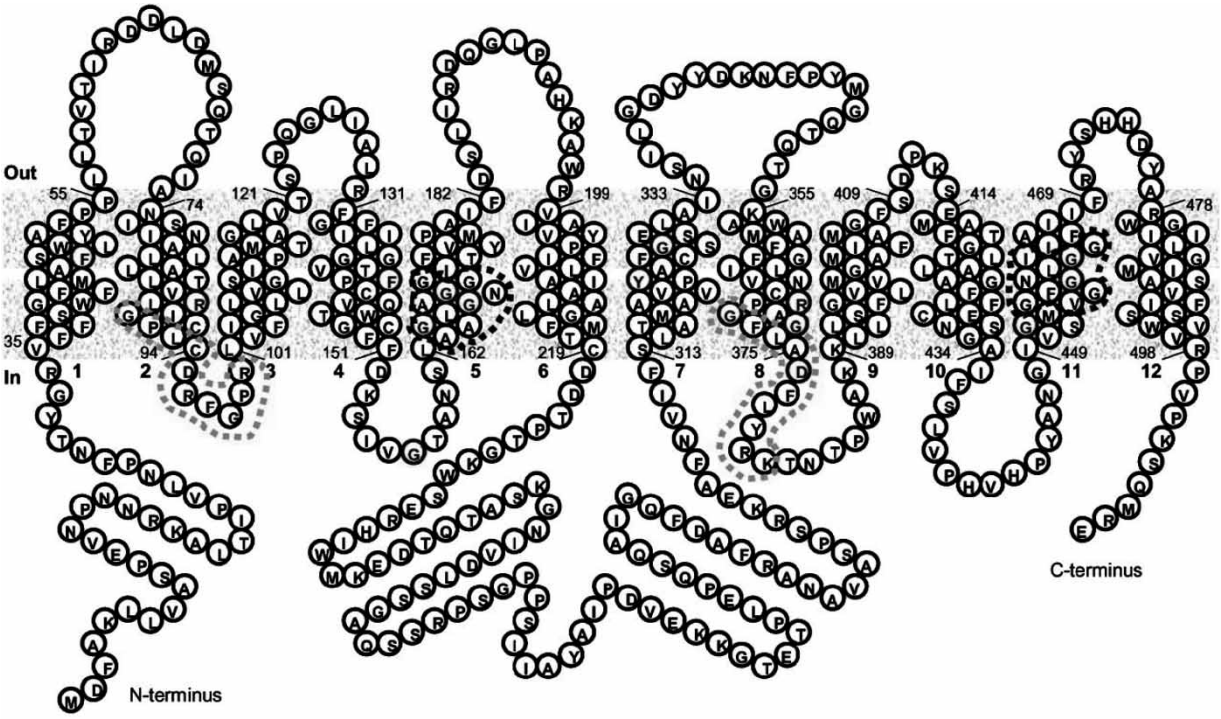

FIGURE 7 Secondary structure model of the NRT, *NrtA* permease of *Aspergillus nidulans*. Residues indicated as faded spheres are highly conserved (>95%) in the NNP family (out, periplasm; in, cytoplasm). The numbers 1–12 on the cytoplasm side of the membrane represent the α-helices (Refs. 55).

a cytoplasmic ATPase (NrtD). NrtA binds nitrate and nitrite ($K_d = 0.3$ mM) [54] and scavenges nitrate/nitrite from the periplasm for the delivery to the permease, NrtB. NrtA also confers nitrate/nitrite specificity on the transporter NrtABCD. The passage of solute through the transmembrane pore is linked to ATP hydrolysis by NrtC and NrtD. NrtD consists of an ATPase domain, whereas NrtC has an ATPase domain and a C-terminal solute-binding domain. The C-terminal solute-binding domain shares 50% sequence similarity with NrtA and is required for the post-translational inhibition of nitrate transport [49,58–60].

The crystal structure of NrtA from *Synechocystis* sp. 6803, complexed to NO_3 and determined to 1.5 Å resolution (Fig. 9) [54], reveals an (α/β protein composed of two domains with a C-clamp shape that forms a solute-binding cleft (Fig. 9). NrtA belongs

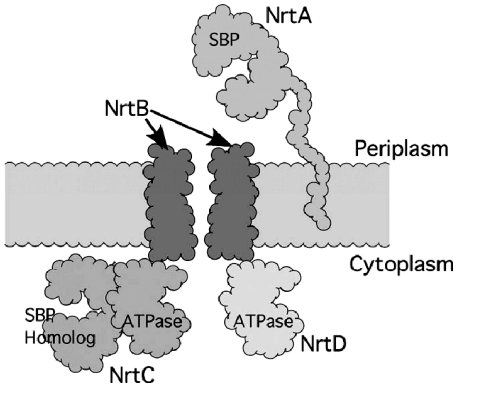

FIGURE 8 Cartoon representation of the assembled NrtABCD NRT showing the orientations of the A, B, C and D components in the periplasmic membrane. NrtA, possessing a 'C-clamp' shape, is tethered to the membrane by a flexible linker and captures NO_3^-/NO_2^- in the periplasm for delivery to the transmembrane complex created by NrtB, NrtC and NrtD. ATPases couple ATP hydrolysis to NO_3^-/NO_2^- transport through the pore. NrtC differs from NrtA in that it has a C-terminal solute-binding domain similar to that of NrtA. [Koropatkin *et al.* [54] *Proc. Natl. Acad. Sci.* **2006**, *103*, 9820–9825. © 2006 National Academy of Sciences, USA].

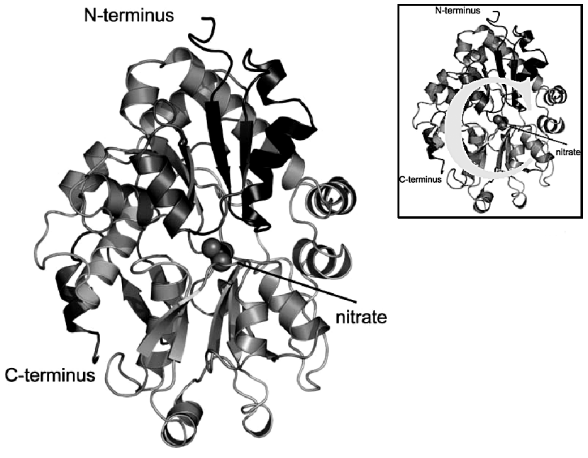

FIGURE 9 Ribbon representation of the crystal structure of NrtA *Synechocystis* 6803. The protein is coloured by gradient from blue to red as the chain extends from the N-terminus to the C-terminus. NrtA consists of two α/β domains shaped like a C-clamp (inset). The view shows the front of the C-clamp, revealing the solute-binding cleft. Nitrate is bound in the cleft between domains. [Koropatkin *et al.* [54] *Proc. Natl. Acad. Sci.* **2006**, *103*, 9820–9825. © 2006 National Academy of Sciences, USA].

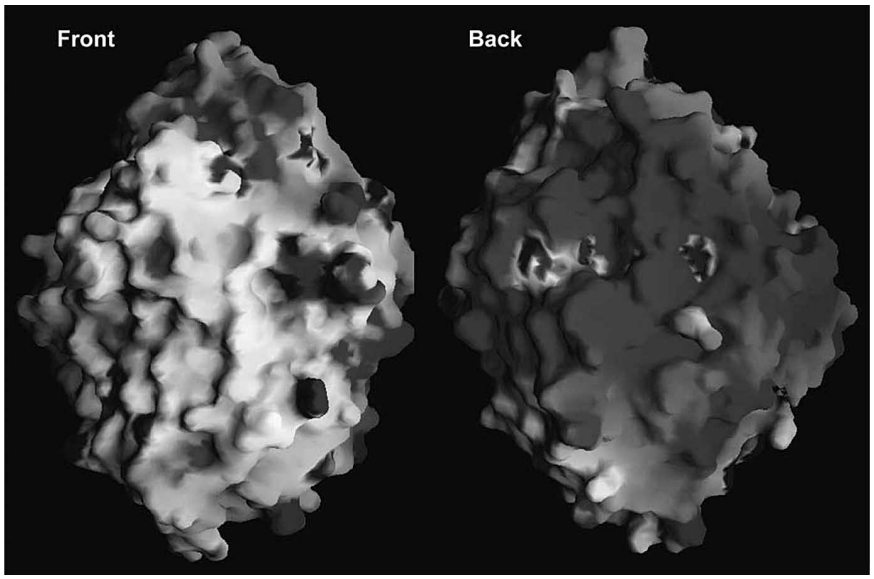

FIGURE 10 The electrostatic surface potential of the front and back of the NrtA structure shows the negative and positive charges as variegated patches. [Koropatkin *et al.* [54] *Proc. Natl. Acad. Sci.* **2006**, *103*, 9820–9825. © 2006 National Academy of Sciences, USA].

to the same superfamily as the phosphate, sulphate and molybdate-binding proteins, where the binding cleft is also sandwiched between the two domains. NrtA has extra amino acid residues forming multiple α-helices and an antiparallel β-sheet extending from the C-terminus. The amino acid extension in NrtA cradles the back of the C-clamp to provide structural support for the nitrate-binding pocket and/or to allow conformational changes associated with NO_3^-/NO_2^- transport.

The electrostatic potential of NrtA is asymmetric, with its back enveloped in negative charge (Fig. 10). The asymmetric charge and the protein's flexible tail may act to prevent unproductive interactions with the membrane and to facilitate association of NrtB and NrtA (Figs. 8 and 10).

One NO_3^- is bound per NrtA [54,61]. As shown in Fig. 11(A), NO_3^- is surrounded by hydrophobic residues lining the entrance of the binding site: Leu 71, Pro 222 and Val 239. Nitrate is thus occluded from interactions with solvent. Nitrate's D_{3h} symmetry is lost due to this asymmetric pocket (Fig. 11(B)). The anion is bound using electrostatic and hydrogen bonds within the cleft such that oxygen O1 of NO_3^- is close to positive charges from K269 and H196 (2.8 and 3.0 Å, respectively) and is 2.9 Å from the N of 55. In contrast, nitrate's O2 is surrounded by the hydrophobic side chains of P222 and V239 and

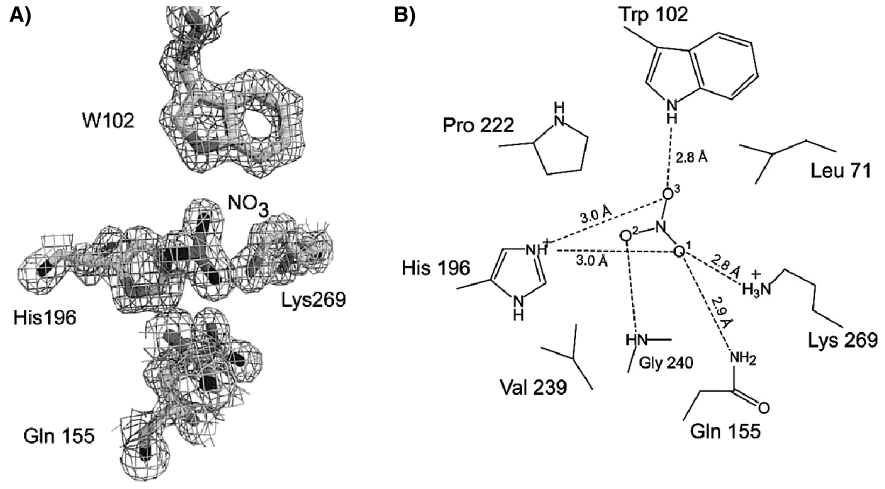

FIGURE 11 (A) Representative electron density of nitrate and coordinating residues in the nitrate-binding cavity of NrtA. G240 was omitted for clarity. (B) Schematic of the nitrate-binding site. The protein–ligand interactions between NrtA and NO_3^- are shown along with all potential hydrogen bonding and electrostatic interactions depicted as dashed lines. The D(H)···O(NO_2) distances in angstrom (Å) for significant interactions are shown. [Koropatkin *et al.* [54] *Proc. Natl. Acad. Sci.* **2006**, *103*, 9820–9825. © 2006 National Academy of Sciences, USA].

weakly bonded to the G240 amide NH. Lastly, nitrate's third oxygen, O3, is hydrogen bonded to W102 (2.8 Å) and is 3.0 Å from H196. This polarises nitrate's charge distribution such that O1, involved in the greatest number of interactions, has a greater negative charge than the other oxygens. This asymmetric environment in the binding cleft may account for why NrtA binds NO_3^- and NO_2^- with similar affinity [($K_d = 0.3$ mM; 61)]. If O1 and O3 interactions remain the same, then NO_2^- can bind to NrtA in a manner similar to nitrate [54].

Smith compared NrtA with the homologous bicarbonate receptor, CmpA [54,60], by aligning sequences and comparing putative binding pockets. The most significant difference between NrtA and CmpA is the substitution of NrtA Lys 269 with a Glu in CmpA. The Lys269 residue in NrtA complements nitrate's negative charge and polarises the anion (Fig. 11(B)). The substitution to Glu would nullify anion binding due to charge repulsion between nitrate and carboxylate. Conversely, the Glu residue provides a hydrogen bond acceptor for the hydroxyl of HCO_3^- in CmpA. Smith proposed that the determining factor for anion selectivity is the charge at residue 269. A crystal structure of CmpA supports this hypothesis [60]. Similar examples of substrate discrimination, based on the deletion or insertion of a hydrogen bonding acceptor, have been observed [62].

Nitrate Reductases

NR reduce NO_3^- to NO_2^-:

$$NO^-_{3(aq)} + 2H^+_{(aq)} + 2e^-_{(aq)} \rightarrow NO^-_{2\,(aq)} + H_2O_{(l)}$$

$$E^\circ = 420\,\text{mV}.$$

NR enzymes are classified according to source, cell localisation and function [43,63]. All NR have a molybdenum cofactor (Moco) and belong to the DMSO reductase family (prokaryotic) or sulphite oxidase family (eukaryotic) [63–65]. Prokaryotic NR enzymes are classified into three groups: respiratory nitrate reductases (Nar), periplasmic nitrate reductases (Nap) and assimilatory nitrate reductases [(Nas; 43,63)].

Mechanism of NO_3^- Reduction by NR

Mechanisms to reduce NO_3^- are similar for NR enzymes. One NAD(P)H unit is used as an electron source for each NO_3^- [66,67]. A hypothetical pathway for NO_3^- reduction is shown in Scheme 3 [65,66]. The NR catalyses a two-electron transfer from NADH or NADPH to FAD and subsequently to Moco. Electrons are transferred through reductive elimination to form NO_2^-. Reduction of NO_3^- is initiated at the reduced Mo^{IV} (**1**, Scheme 3). The NO_3^- binds to Mo, releasing hydroxide (**2**, Scheme 3). Oxidation of Mo^{IV}–Mo^{VI} initiates bond breaking between nitrate's oxygen and nitrogen to generate NO_2^- (**3**–**5**, Scheme 3). The Mo^{IV} is regenerated by a two-electron transfer from NAD(P)H [65].

No crystal structures exist for the Nas [63]; crystal structures of Nar and Nap families are known [65–70]. But, these structures do not contain NO_3^- [65–70]. Thus, interactions of NO_3^- with NR remain speculative. Schwarz and co-workers have simulated the position of NO_3^- in an NR active site [65]. They grew crystals of two recombinant species expressed from nitrate-reducing molybdenum (NR–Mo) fragment of yeast. Crystal structures revealed four ordered waters in the active site [65]. The orientation of three waters mimicked what NO_3^- might adopt if bound. They modelled NO_3^- into the active site by superimposing the anion over bound waters. Two waters formed hydrogen bonds with two arginines and one tryptophan (Fig. 12(A)). Superimposing NO_3^- resulted in hydrogen bonds between NO_3^- and

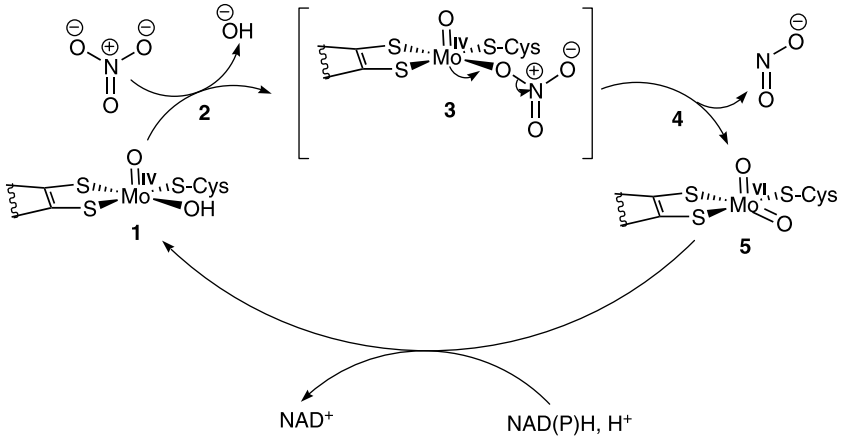

SCHEME 3 The proposed catalytic cycle of NO_3^- reduction by the Moco domain of NR utilising NAD(P)H as the electron source. The different stages of the cycle are labelled **1**–**5**. [Fischer *et al.* [65] *Plant Cell* **2005**, *17*, 1167–1179. www.plantcell.org © 2005 American Society of Plant Biologists].

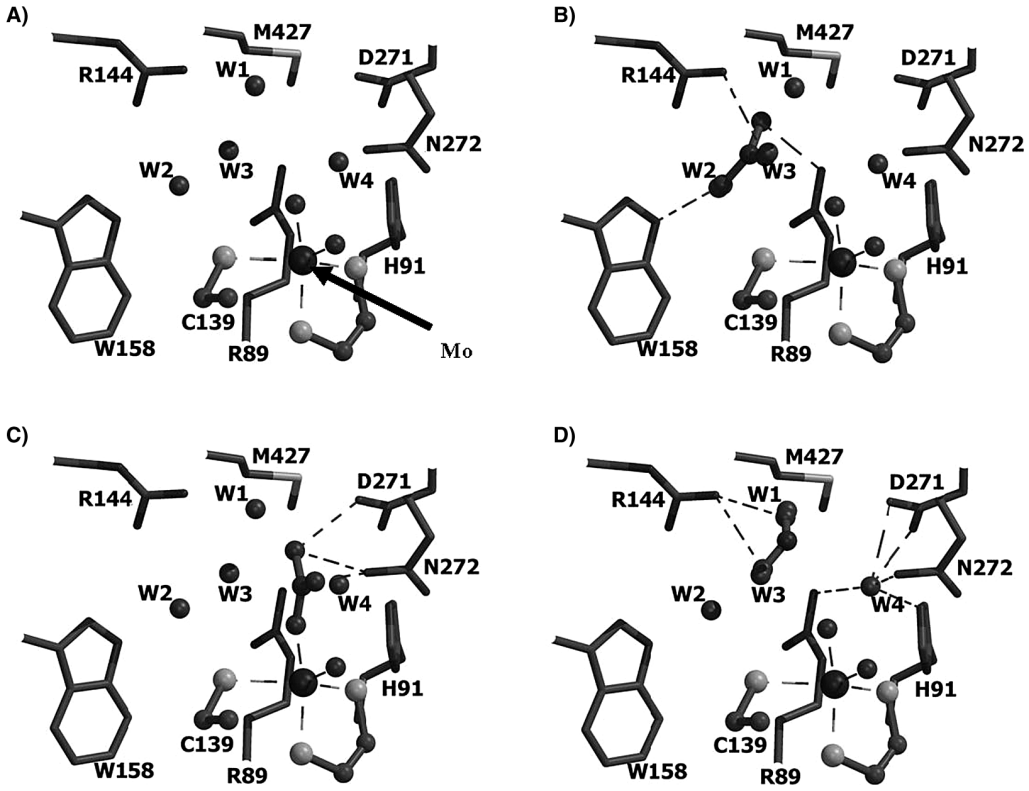

FIGURE 12 (A) Model of the active site of one of the recombinant NR showing the Mo centre and the four water molecules (W1–W4) bound to the enzyme as seen in the crystal structure. (B) Modelled NO_3^- is superimposed over W2 and W3 to simulate NO_3^- binding in the active site. (C) Nitrate's approach to the metal centre. (D) Release of NO_2^- after reduction. Interacting centres are shown as spheres and the amino acid residues as stick models. [Fischer *et al.* [65] *Plant Cell* **2005**, *17*, 1167–1179. www.plantcell.org © 2005 American Society of Plant Biologists].

these residues (Fig. 12(B)) [65]. Since modelling NO_3^- into the active site provided a good fit, the mechanism of NO_3^- reduction was proposed. The model in Fig. 12(C) shows the approach of NO_3^- to the metal and formation of hydrogen bonds with Asp271 and Asn272. The NO_3^- displaces bound hydroxide and is reduced after coordination to amino acid residues and Mo. The released NO_2^- is superimposed on water 1 and 2 and bound to Arg144 (Fig. 12D).

SYNTHETIC RECEPTORS FOR NITRATE

Nitrate receptors have incorporated neutral and/or charged groups. We discuss such receptors, especially for which crystal structures are available. We also discuss coordination compounds as cores for NO_3^- receptors.

Pyrrole-based Receptors

Calix[*n*]pyrroles are potent anion binders [21]. Their selectivity can be adjusted by varying substitution and ring size (Scheme 4) [71,72]. To date, there is no NO_3^--selective calix[*n*]pyrrole. The stability of the 1:1 complexes between pyrrolic receptors and anions is related to receptor acidity and anion basicity [73]. Since NO_3^- is weakly coordinating, it may not form strong complexes with calix[*n*]pyrroles. Also, calix[*n*]-pyrroles have small cavities that may disfavour the inclusion of NO_3^-.

Calix[*n*]bis(pyrrole-2-yl)benzenes (calix[*n*]BPBs) incorporate benzene rings into the scaffold, resulting in larger cavities than calix[*n*]pyrroles, while retaining the same number of hydrogen bond donors (Scheme 5). Pyrrolic hydrogens are farther apart,

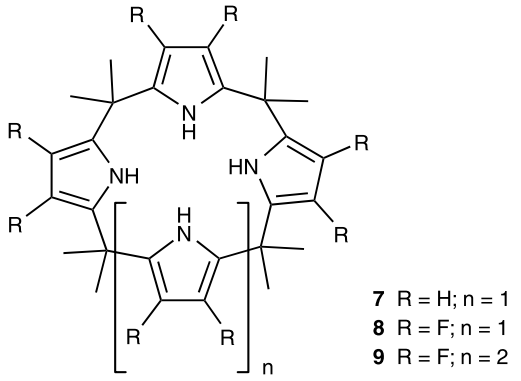

SCHEME 4 Examples of calix[*n*]pyrroles and their anion selectivity: calix[*4*]pyrrole *7* selective for F^-, octa-fluorinated calix[*4*]pyrrole **8** selective for Cl^- and deca-fluorinated calix[*5*]pyrrole **9** selective for acetate (Refs.; 71,72).

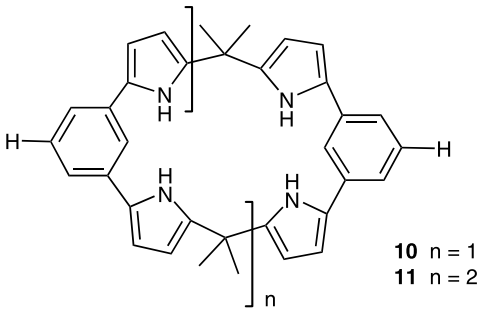

SCHEME 5 Calix[*n*]bispyrrolylbenzenes are analogous to calix[*n*]pyrroles in the number of hydrogen bond donors but differing in the directionality of the hydrogen bonds. Calix[2]bispyrrolylbenzene **10** is analogous to calix [4] pyrrole **7**, while calix[3]bispyrrolylbenzene **11** is analogous to calix[5]pyrrole. [Sessler *et al.* (22) *Chem. Eur. J.* **2005**, *11*, 2001–2011. © Wiley-VCH Verlag GmbH & Co. KGaA. Reproduced with permission].

TABLE I Anion-binding constants (M^{-1}) for pyrrole-based receptors **7**, **10** and **11** obtained in CD_2Cl_2 by ^1H NMR*

Anion	Calix[4]pyrrole **7**	Calix[2]BPB **10**	Calix[3]BPB **11**
F^-	17,000	> 10,000	> 10,000
Cl^-	350	> 10,000	3100
Br^-	10	> 10,000	390
I^-	<10	> 10,000	150
HSO_4^-	<10	> 10,000	850
$H_2PO_4^-$	97	6300	1700
NO_3^-	<10	> 10,000	5100

*Anions used as their tetrabutylammonium salts; n.d., not determinable. [Sessler *et al.* [71], *Chem. Eur. J.* **2005**, *11*, 2001–2011. © Wiley-VCH Verlag GmbH & Co. KGaA. Reproduced with permission].

changing the directionality of the receptor–ligand hydrogen bonds [74]. Also, the benzene rings may form C—H hydrogen bonds, providing enhanced anion affinity [26,27]. Calix[2]bispyrrolylbenzene (calyx[2]BPB) **10** binds anions, including NO_3^-, with greater affinity than calix[4]pyrrole **7** (Table I). The structure of calix[2]BPB **10** with NO_3^- shows that the calix[2]BPB adopts a cone conformation and binds NO_3^- through N—H···O hydrogen bonds (Fig. 13) [74]. Calix[2]BPB coordinates two of nitrate's three oxygens, such that one of the coordinating oxygens is bound to three NH protons, while the other oxygen is bound to the last NH (Fig. 13). Hydrogen bond distances (N—H···O) are 2.09–2.56 Å and N—H···O bond angles are 160–175°. Aryl protons (H_a) on the benzene also form hydrogen bond with the anion. Unfortunately, this receptor is not selective, as the binding constants are $> 10{,}000\,M^{-1}$ in CD_2Cl_2 for most anions (Table I) [74].

On the other hand, expanding the macrocyclic ring of calix[2]BPB **10** by one unit to give calix[3]bispyrrolylbenzene **11** (Scheme 5) reduces anion-binding affinity but increases selectivity. In CD_2Cl_2, calix[3]-BPB **11** still binds fluoride with $a > 10{,}000\,M^{-1}$ binding constant; however, the binding constant for other anions decreases. Macrocycle **11** binds NO_3^- ($5100\,M^{-1}$) and Cl^- ($3100\,M^{-1}$) strongly, but I^-, Br^-, HSO_4^-, $H_2PO_4^-$ and $C1O_4^-$ are bound marginally. The solid-state structure reveals that the expanded **11** folds into a V-shape and forms hydrogen bond with all three NO_3^- oxygen atoms, using four of its six pyrrole NH protons. Calix[3]BPB **11** forms hydrogen bond with each oxygen with distances (N—H···O) between 2.32–2.51 Å and N—H···O bond angles of 167–172° (Fig. 14) [74]. Hydrogen bonds in macrocycles **10** and **11** show properties that are close to ideal for NO_3^- coordination [30].

Another class of polypyrrolic macrocycles described by Sessler and co-workers portrays how subtle variations in structure can influence anion-binding affinity/selectivity. The 2,5-diamidothiophene bipyrrole Schiff-base macrocycles **12** and **13**

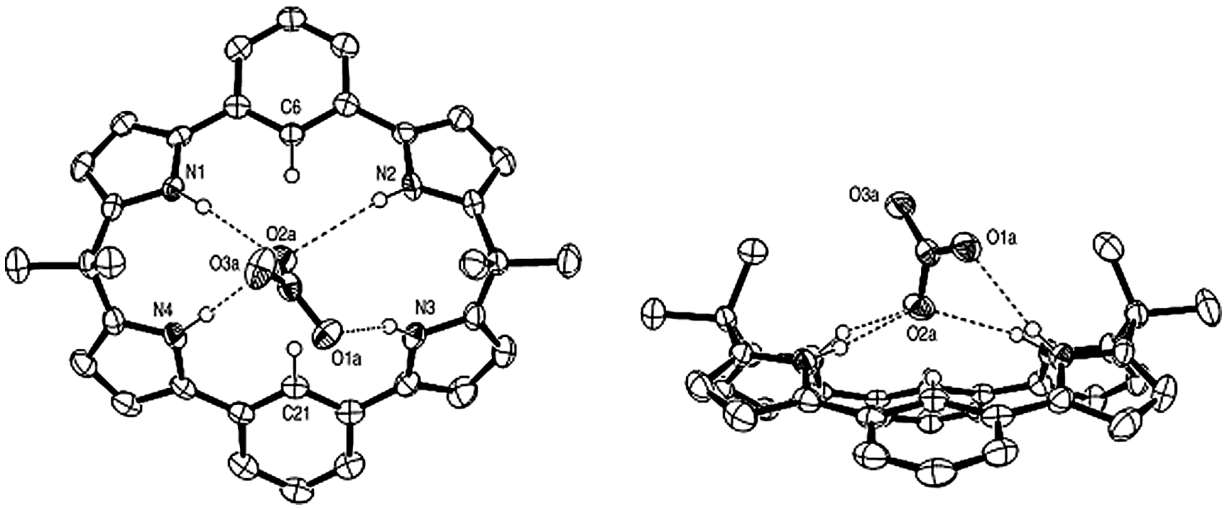

FIGURE 13 X-ray crystal structure of calix[2]bispyrrolylbenzene **10** bound to NO_3^- showing the hydrogen bond contacts between nitrate's oxygen atoms and the pyrrole NH donors. [Sessler *et al.* [71] *Chem. Eur. J.* **2005**, *11*, 2001–2011. © Wiley-VCH Verlag GmbH & Co. KGaA. Reproduced with permission].

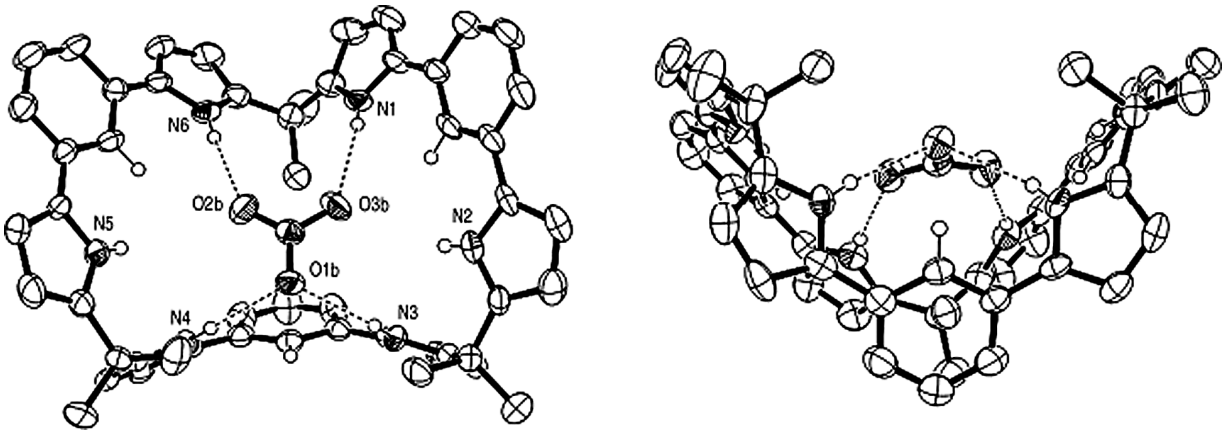

FIGURE 14 Crystal structure of calix[3]bispyrrolylbenzene **11** bound to NO_3^- showing the top (left) and side (right) views. The macrocycle folds and adopts a V-shape to bind nitrate. All three NO_3^- oxygens form hydrogen bond with the macrocycle. [Sessler *et al.* [71] *Chem. Eur. J.* **2005**, *11*, 2001–2011. © Wiley-VCH Verlag GmbH & Co. KGaA. Reproduced with permission].

differ in structure in the linkage between the pyrrole rings, resulting in **12** being more flexible and **13** being rigid (Scheme 6) [22]. The X-ray crystal structure of macrocycle **12** (bound to several acetone molecules) reveals a conformation in which the orientation of the sulphur atom of the thiophene and the pyrrolic NH groups is disordered [22]. This disorder was attributed to the flexible dimethyl methylene linker of the bipyrrole unit. In contrast, the crystal structure of **13** reveals a more rigid framework in which 'the bipyrrole unit forces the macrocycle to adopt an "all-in" structure such that all of the N and S atoms point in towards the centre of the ring' [22]. The disorder in the structure of macrocycle **12** results in a crowded, smaller cavity compared with the larger and more rigid cavity of **13**. The anion binding of the macrocycles **12** and **13** was investigated in dichloroethane using UV–vis spectrophotometric titrations. In general, macrocycle **12** displays a higher affinity for the anions studied, with preference for anions with smaller volumes (Cl^-, NO_3^- and HSO_4^-) regardless of geometry (Table II). Macrocycle **13**, however, interacts more strongly with the larger anions considered in the study. Thus, the inference is that the rigid and well-defined cavity of macrocycle **13** prevents it from interacting with or accommodating anions of smaller dimensions and higher charge densities [22].

Amide-based Receptors

The amide group is used by proteins to bind NO_3^- [54,65]. Synthetic chemists have also incorporated amides into anion receptors [3,75,76]. Anslyn reported an amide-linked C_3-symmetric bicyclic cyclophane **14** that bound NO_3^- and $CH_3CO_2^-$ with high affinities [77]. A crystal structure revealed that acetate is bound inside the bicyclic cavity (Fig. 15). Each acetate oxygen forms hydrogen bond with two hydrogens from the same acyl pyridine group on two of the cyclophane's three corners (Fig. 15). Crystallographic evidence for **14** bound to NO_3^- was

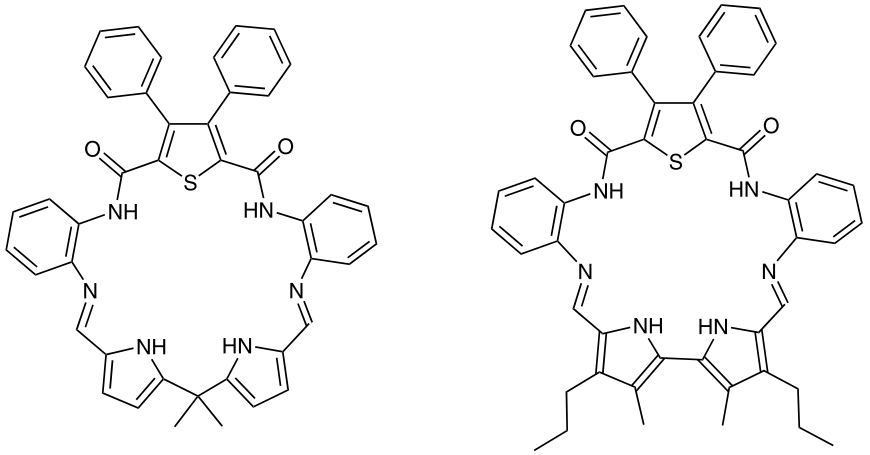

12 **13**

SCHEME 6 Calix[2]benzopyrrole **12** and **13**. [Reprinted with permission from [22] Copyright © 2005 American Chemical Society].

TABLE II Anion-binding constants (M^{-1}) for bipyrrole receptors **12** and **13** obtained in CH_4Cl_2 and determined by UV–vis spectroscopic titrations

Anion	12	13	Anion volume (Å^3)
Cl^-	16,600 ± 900	3300 ± 300	24.8
Br^-	7100 ± 1000	7100 ± 900	31.5
AcO^-	3200 ± 600	3600 ± 300	17.8
NO_3^-	15,400 ± 2100	1000 ± 300	24.0
HSO_4^-	18,900 ± 1000	7400 ± 800	28.7
$H_2PO_4^-$	9500 ± 400	[a]	33.5

[a] Could not be fitted to the binding profile. 1:1 Binding stoichiometries used. Anions studied as their tetrabutylammonium salts. (Reprinted with permission from [22] Copyright © 2005 American Chemical Society].

not obtained. Anslyn concluded that NO_3^- is bound to **14** similarly to acetate since NO_3^- is also planar and bound only 2.6 times less strongly ($K_a \approx 300$ and 770 M^{-1} in CD_2Cl_2/CD_3CN (1:1 v/v) for NO_3^- and $CH_3CO_2^-$), even though $CH_3CO_2^-$ is 10^6 more basic [77]. The selectivity for NO_3^- by cyclophane **14** is enhanced as solvent polarity decreases [78].

Smith and co-workers [20,79–81] have developed ditopic receptors for ion pair binding. Receptor **15** consists of cation (crown ether) and anion (isophthalamide) binding sites (Fig. 16) and binds anions of different geometries in polar and nonpolar solvents. Crystal structures of receptor **15** bound to NO_3^- with different cations (Li^+, Na^+, K^+) were reported [20]. The cation is important for binding geometries. The complex between **15** and $K^+ + NO_3^-$ shows that two of the NO_3^- oxygens chelate the cation and the third is hydrogen bonded to amide NH (Fig. 17(A)). Two hydrogen bonding contacts of nitrate's third oxygen with the receptor's amide NH protons are such that one of the interactions is stronger than the other. In this 15 $K^+ \cdot NO_3^-$ complex, the NO_3^- is situated further outside the cavity and is positioned asymmetrically with respect to the two amides. This makes one hydrogen bonding interaction moderately strong (N···O, $d = 2.90$ Å) and the other nonexistent (N···O, $d = 3.84$ Å). Similar, hydrogen bonding and electrostatic interactions are observed for the 15·$Na^+ \cdot NO_3^-$ complex. However, the third oxygen in the Na^+ complex is situated farther away (3.14 and 3.24 Å) from the two amide nitrogens in a nearly equidistant fashion (Fig. 17(B)). When the smaller lithium cation is incorporated, significantly different interactions are observed. The NO_3^- in 15·$Li^+ \cdot 2H_2O \cdot NO_3^-$ does not directly coordinate Li^+, but rather associates with the cation via a bridging water molecule (Fig. 17(C)). Only one of the NO_3^- oxygens is coordinated in the complex. This oxygen points inside the cavity to form hydrogen bond with both amide NH protons and the bridging water molecule. The hydrogen bond from water is directed at nitrate's π-electron cloud rather than at oxygen lone pairs [20]. These interactions affect the geometric alignment of the NO_3^- in the complex. In the 15·$Na^+ \cdot NO_3^-$ and 15 $K^+ \cdot NO_3^-$ complexes, the NO_3^- is approximately parallel to the host's hydrogen bond donors. However, in the 15·$Li^+ \cdot 2H_2O \cdot NO_3^-$ complex, the NO_3^- is situated almost perpendicular to the NH hydrogen bond donors and coplanar with the crown ether. Data presented in Table III are for N···O distances, and N—H···O bond and H···O—N—O dihedral angles for the interactions of receptor **15** with NO_3^-. The N···O distances indicate that the hydrogen bonds are all of moderate strength and the N—H···O bond angles are within the range for favourable NO_3^- coordination [30].

Another, noteworthy example of an amide-based NO_3^- receptor is cyclic triamide **16** (Scheme 7). Although a crystal structure of **16** bound to NO_3^- was not obtained, the association constant for the **16**·NO_3^- 1:1 complex in DMSO is one of the highest reported [($K_a = 110\ M^{-1}$ in 50% DMSO-d_6/$CDCl_3$ or 20 M^{-1} in 100% DMSO-d_6; 82)].

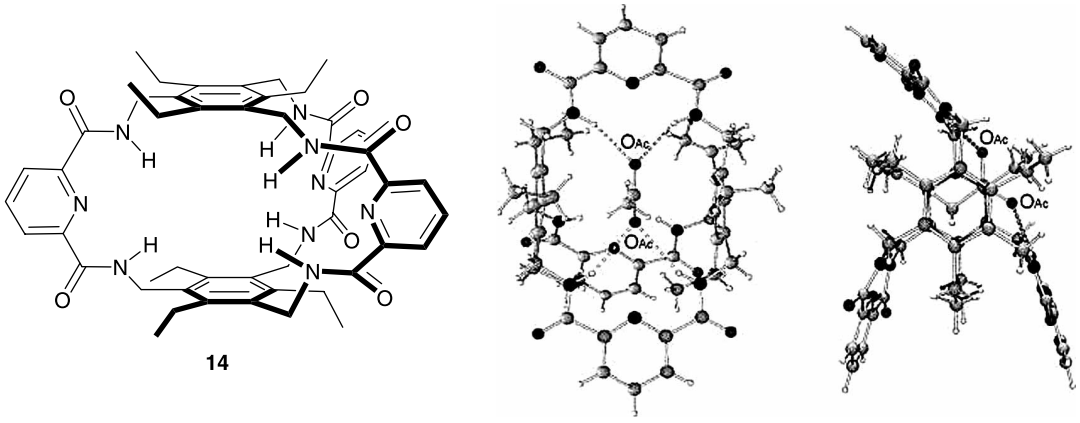

FIGURE 15 Schematic of bicyclic cyclophane **14** (left) and two views of the crystal structure of **14** bound to $CH_3CO_2^-$ (centre and right) showing hydrogen bonds between the acetate and the amide NH protons of the cyclophane. There appears to be weak van der Waals interactions between two of the three CH_3 protons of acetate and the two triethylbenzene rings of **14**. [Reprinted with permission from ref. [76] © 2006 Elsevier].

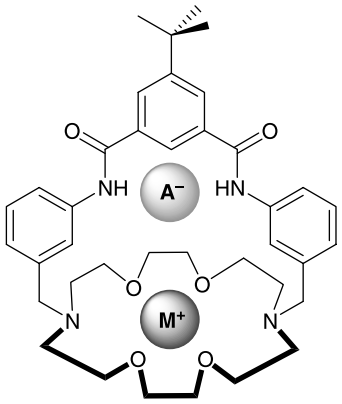

15

FIGURE 16 A schematic of the ditopic receptor **15**. [Reprinted with permission from [20] Copyright © 2005 American Chemical Society].

Ammonium-based Receptors

Polyammonium macrocyclic receptors are among the most widely studied hosts for anion complexation because of the strength and stability of the host–guest complexes. Both electrostatic and hydrogen bonding interactions govern binding between the receptors and the anions. García-España [83] and Bowman-James [84] have reviewed ammonium-based anion receptors. Bowman-James [84] presented examples of polyammonium macrocycles that bind NO_3^- in solution and the solid state. The trend from the crystallographic data of polyammonium macrocycles is that bound NO_3^- does not reside within the cavity, but hovers out of the plane of the planar macrocycles [84–86]. To encapsulate NO_3^-, Bowman-James and co-workers [87] hypothesised that bicyclic polyammonium macrocycles

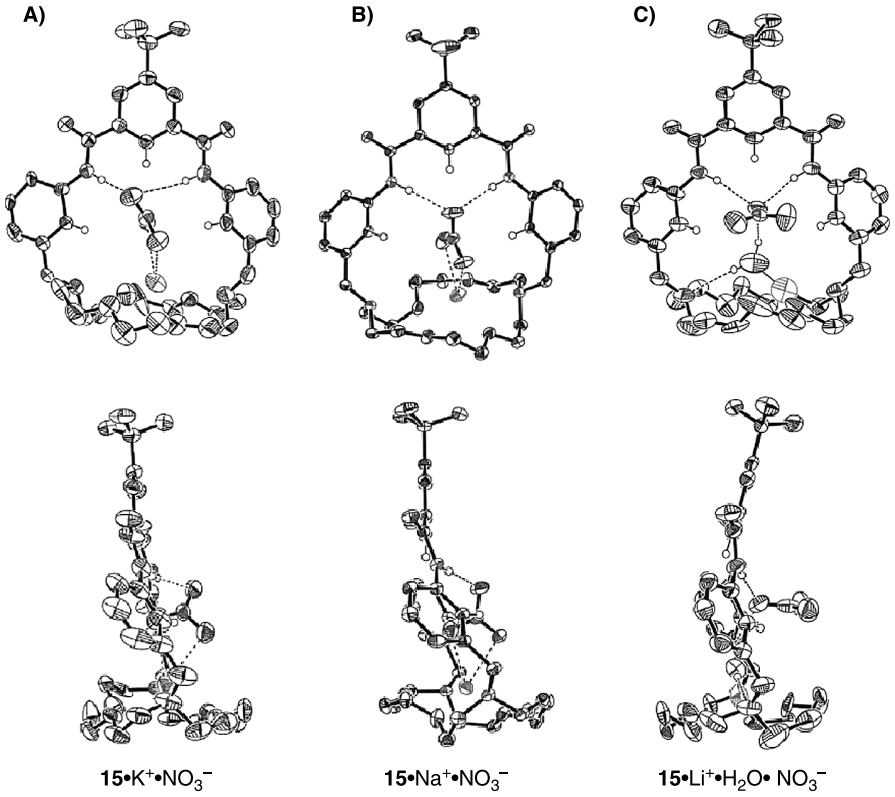

FIGURE 17 Crystal structures of the complexes of the ditopic receptor **15** with NO_3^- and alkali metal ions (A) **15**$K^+ \cdot NO_3^-$, (B) **15**$\cdot Na^+ \cdot NO_3^-$ and (C) **15**$\cdot Li^+ \cdot 2H_2O \cdot NO_3^-$. The Li^+ complex incorporates two water molecules. The water molecule located underneath the crown and coordinated to the Li^+ is not shown. The orientation/position of NO_3^- relative to the receptor's cavity changes depending on the cation. [Reprinted with permission from [20] Copyright © 2005 American Chemical Society].

TABLE III Selected solid-state data for receptor **15**'s NH···anion interactions

	H···O—N—O dihedral angles (°)	N···O distance (Å)	N—H···O angles (°)
15·$NaNO_3$	78	3.145	176
	34	3.235	177
15·KNO_3[a]	70	3.836	166
	15	2.903	160
15·$Li \cdot 2H_2O \cdot NO_3$	37	3.070	169
	28	3.031	170

[a] Data for 70% occupancy. [Reprinted with permission from [20] Copyright © 2005 American Chemical Society].

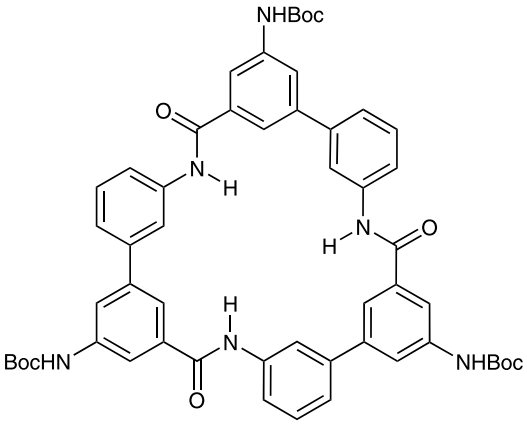

SCHEME 7 Cyclic triamide **16**. [Reprinted with permission from [82] Copyright © 2003 American Chemical Society].

with C_3-symmetry might be more effective in binding the trigonal anion.

The 28-membered cyclam-based macrocycle (**17**; Fig. 18(A)) containing amide and ammonium functionalities binds both Cu^{2+} and NO_3^- [19]. Structural analysis of the complex of **17** with NO_3^- revealed that the macrocycle is tetra-protonated, adopts a rectangular shape and possesses a hollow cavity occupied by two NO_3^- ions (Fig. 18(B)). The NO_3^- ions are pressed against the macrocycle's two walls putting them in close proximity to two ammonium (NH_2^+) moieties. The distances between NO_3^- and the NH_2^+ groups are 2.72–2.98 Å, with each NO_3^- participating in two hydrogen bond interactions. The two NO_3^- ions in the macrocyclic cavity are arranged in a staggered conformation with respect to each other. The macrocycles are stacked in a staggered arrangement, allowing hydrogen bonding between carbonyl oxygens of one macrocycle and amide NH protons of neighbouring macrocycles (Fig. 19(A)). This stacking is similar to the hydrogen-bonded arrangement found between adjacent peptide chains in β-sheet proteins [19,88]. A view down the axis of the stacked macrocycles reveals a channel filled by NO_3^- (Fig. 19(B)).

Bowman-James and co-workers [87] isolated crystals of the nitrate complex of bicyclic azacryptand **18**. The cryptand is C_3-symmetric and crystallography revealed two NO_3^- ions encapsulated in the

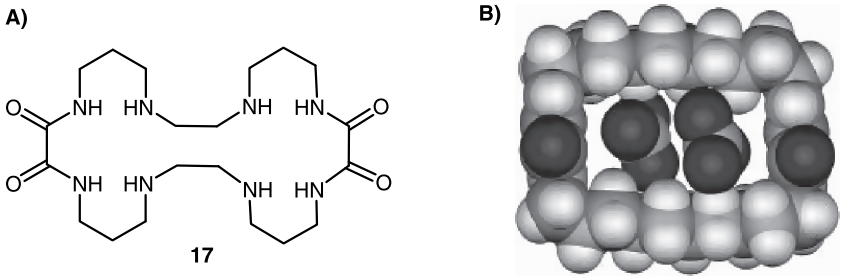

FIGURE 18 (A) ChemDraw structure of macrocycle **17**. (B) Space-filling representation of the crystal structure of the protonated [**17**H_4·$(NO_3^-)_4$] macrocycle. The view shows the macrocycle with the two NO_3^- ions included in the cavity. [Reprinted with permission from [19] Copyright © 2004 American Chemical Society].

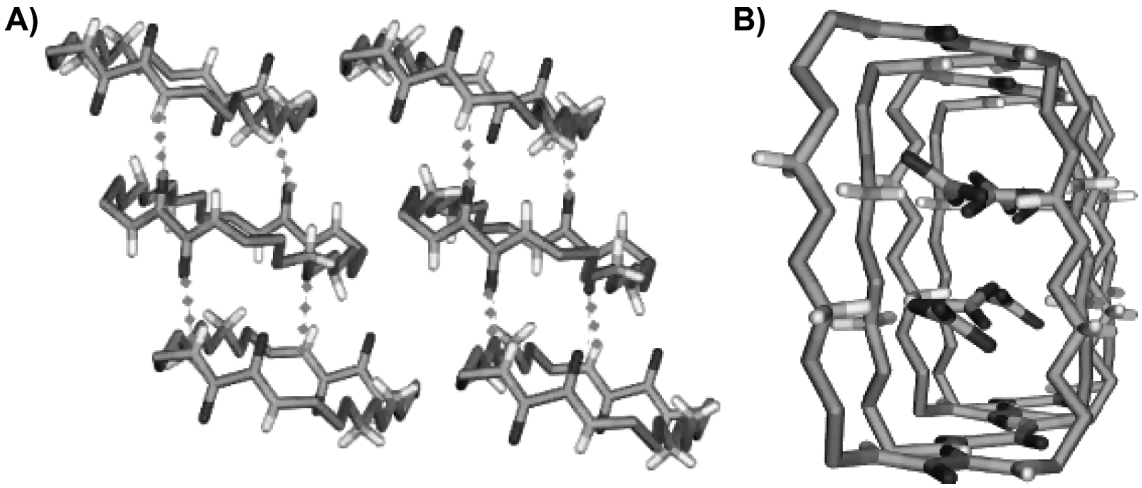

FIGURE 19 (A) Representation of the solid-state packing arrangement of macrocycle **17**. Hydrogen bonds between the stacked macrocycles are depicted as dotted lines. (B) Representation of the solid-state packing arrangement of **17** viewed to show the channel-like pore with the encapsulated NO_3^- ions. [Reprinted with permission from [19] Copyright © 2004 American Chemical Society].

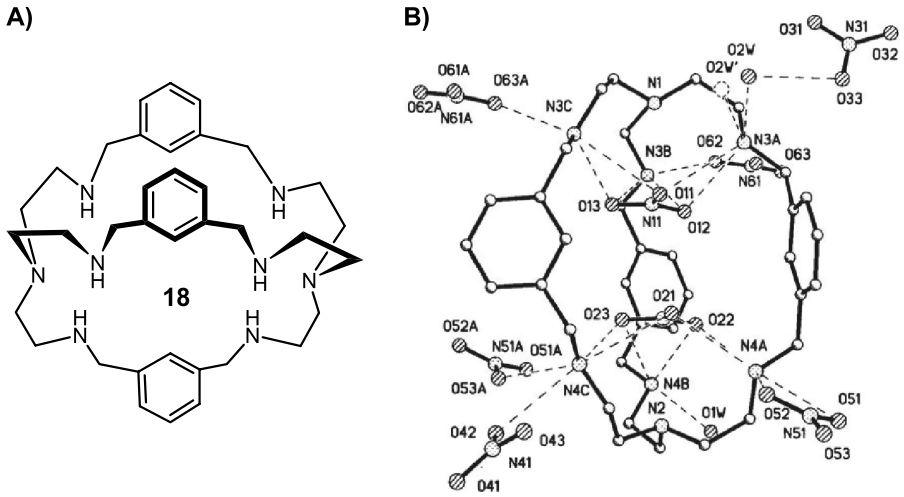

FIGURE 20 (A) ChemDraw structure of azacryptand **18**. (B) Hexa-protonated **18** with two nitrate ions (N11 and N21) bound within the bicyclic cavity. Bifurcated hydrogen bonds and the other associated nitrate ions and water molecules are also shown [89]. *Reproduced by permission of The Royal Society of Chemistry (RSC).*

bicyclic cavity of **18** (Fig. 20). Cryptand **18** has six NH_2^+ groups, two from each arm pointed towards the cavity. The cryptand is bound to six NO_3^- ions: two ions within the cavity and four others bound outside the cavity [(N31, N41, N51 and N61 in Fig. 20(B); *89*)]. Surprisingly, the two encapsulated NO_3^- ions are oriented in an eclipsed conformation with a $N_{nitrate}\cdots N_{nitrate}$ distance of 3.34 Å. This short distance might be expected to cause NO_3^-—NO_3^- repulsion (Fig. 21). Theoretical modelling of the cryptand-NO_3^- binding, using the coordinates of the cryptand-NO_3^- structure and the CHARMM program, revealed that the minimised structure and the crystal structure are nearly superimposable [87]. Calculations suggested that the NO_3^--cryptand interaction was stronger than any NO_3^-—NO_3^- repulsion. The interactions of the NO_3^- with the cryptand in the solid state show that each encapsulated NO_3^- forms six hydrogen bonding contacts, in which each nitrate's oxygen makes two hydrogen bonds with separate ammonium NH_2^+ groups (Fig. 20(B)). The hydrogen bonds are not, however, equal in strength. The NO_3^- makes three stronger hydrogen bonds with the host ranging from 1.90 to 2.02 Å and three weaker hydrogen bonds ranging from 2.28 to 2.39 Å.

Solution studies revealed that the cryptand binds NO_3^- in D_2O with an apparent K_a value of $10^3\,M^{-1}$, albeit in a 1:1 model of host–guest binding. The 1:2 host–guest binding model is not favoured in solution [89]. The discrepancy between solution and solid-state results emphasises the fact that X-ray crystallographic evidence does not necessarily depict solution events. It is important to extensively study the solution properties of any receptor system to fully characterise that system. On the other hand, the strength of nitrate binding by cryptand **18** in polar solvents, along with the solid-state evidence that each nitrate oxygen is involved in the maximal/optimal number of bonding contacts [30], underscores the importance of the geometrical complementarity of the host in binding anions, especially weakly coordinating ones such as nitrate.

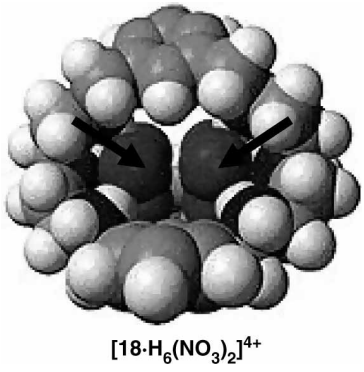

FIGURE 21 The space-filling model of hexa-protonated cryptand **18** shows the two NO_3^- ions (arrows) occupying the pocket in an eclipsed conformation relative to each other. [Reprinted with permission from [87] Copyright © 1998 American Chemical Society].

Urea-based Coordination Compounds

Crystal structures of urea-based receptors bound to NO_3^- are scarce. The examples presented here are those of metal coordination compounds containing the urea moiety. Steed and co-workers reported a class of ditopic receptors containing pyridyl and urea functionalities [24]. The compounds act as ligands for transition metals while retaining their ability to interact with anions. For example, the ureidopyridine ligand **19** reacts with silver nitrate ($AgNO_3$) to give discrete complexes $[Ag(\mathbf{19})_2(S)]NO_3$ **20a** (S (solvent) = MeOH) and **20b** ($S = NO_2Me$) ((Fig. 22) 90). Two ureidopyridyl ligands coordinate the same Ag^+, such

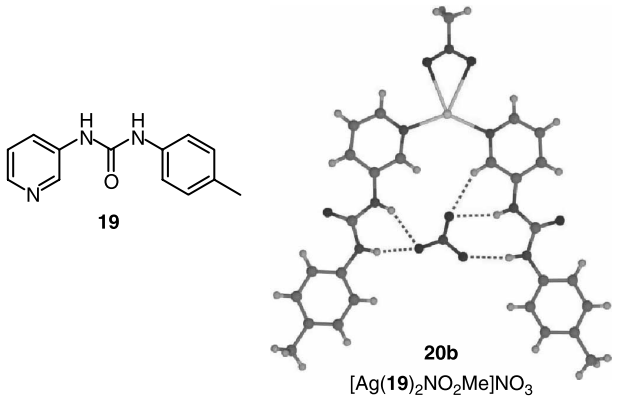

FIGURE 22 Ureidopyridine ligand **19** and the X-ray crystal structure of its nitromethane–silver nitrate complex $[Ag(\mathbf{19})_2NO_2Me]NO_3$ **20b**. In complex **20a**, the nitromethane molecule is replaced by a methanol molecule. Hydrogen bonds are depicted as dashed lines [24,90]. *Reproduced by permission of The RSC* and *on behalf of the Centre National de la Recherche Scientifique (CNRS).*

that the urea hydrogen atoms converge to form a central pocket. A bound NO_3^- is sandwiched between these two ureidopyridyl ligands. In **20a** and **20b**, NO_3^- is chelated by the urea groups from both ligand arms in an off-centre fashion, with **20a** having a higher degree of disorder than **20b** (**20b**, Fig. 22). The offset chelation allows for one CH···O interaction with the pyridyl ring in addition to four NH···O hydrogen bonds from the acidic urea protons [90]. The anion-binding properties of the ligand **19** and its silver complex $[Ag(\mathbf{19})_2]^+$ in solution were studied by ^1H NMR experiments. The association constants were determined in acetonitrile-d_3. The solution results indicated that discrete structures such as **20** were maintained in solution, and bound NO_3^- strongly in 1:1, 1:2 and 1:3 host-to-anion-binding modes (Table IV). The association constant for the 1:3 binding mode (K_{13}), obtained with a large excess of added NO_3^-, is two orders of magnitude less than the 1:1 binding mode and is attributed to the coordination of NO_3^- to the metal centre (Table IV) [90]. As seen from the binding constants in Table IV, NO_3^- anion binding is enhanced in the complexes compared with the free ligand. This is because the effective number of contacts between the urea ligands and the NO_3^- anion is maximised. This arrangement is similar to that in the NR active site. The Mo metal centre binds to the NO_3^- anion, maximising the number of contacts to the anion for catalytic reduction to NO_2^-.

When transition metal nitrates such as $Co(NO_3)_2$, $Ni(NO_3)_2$ and $Cu(NO_3)_2$ are used to form coordination compounds with ligand **19**, a series of 1:4 metal-to-ligand complexes like $[Cu(\mathbf{19})_4(H_2O)_2](NO_3)_2$ **21** are formed (Fig. 23) [24,91]. In the cobalt and nickel complexes, nitrate ions interact with only one urea group per complex, as well as with water and methanol coordinated to the metal centre. Interactions in the Co^{2+} and Ni^{2+} complexes are such that NO_3^- is held by hydrogen bonding between pairs of ligands from adjacent complexes, so that each ligand in a particular complex interacts with a different nitrate anion [91]. In contrast, the coordinated water molecules in copper complex **21** are too far from NO_3^- and do not interfere with the nitrates' chelation to the ligands. Thus, in the Cu^{2+} complex **21**, pairwise interactions of urea groups bound to the metal centre with NO_3^- are formed (Fig. 23). Also, the NO_3^- anions are complexed in a conformation similar to the lowest energy conformation calculated by Hay and co-workers for 2:1 urea–nitrate complexes [34].

Finally, a silver nitrate complex of ligand **22**, the bis(ureidopyridine) analogue of **19**, was characterised. This ligand forms a metallomacrocycle **23**, where two ligand molecules are held together by two silver ions. The urea groups of ligand **23** point outwards from the inner cavity of the macrocycle and are hydrogen bonded to NO_3^-. The hydrogen-bonded NO_3^- serve as bridges between adjacent macrocycles to form a network (Fig. 24) [24,92]. Additional CH···O interactions similar to those in complex **20** help to stabilise the hydrogen-bonded network. The macrocyclic cavity is occupied by two acetonitrile molecules that also coordinate the metal

TABLE IV Binding constants (M^{-1}) obtained by ^1H NMR titrations in CD_3CN for the free ligand **19** and the complex $[Ag(\mathbf{19})_2]^+$

	19		$[Ag(\mathbf{19})_2]^+$	
	K_{11}	K_{11}	K_{12}	K_{13}
NO_3^-	956	30,200[c]	2900	550[c]
$CH_3CO_2^-$	$> 10^5$[a]	4.97×10^5[c]	–[b]	5.31×10^6[c]

[a] Binding constant was too high to be accurately determined. [b] No identifiable 1:2 complex formed. [c] For nitrate, K_{13} represents the coordination of the anion to the metal centre, whereas for acetate K_{11} represents the same process [90]. *Reproduced by permission of The RSC on behalf of the CNRS.*

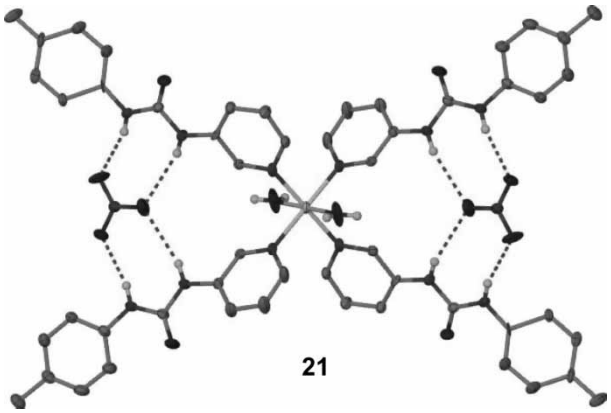

FIGURE 23 The X-ray crystal structure of $[Cu(\mathbf{19})_4(H_2O)_2](NO_3)_2$, **21**. The 1:4 metal-to-ligand complex of the ureidopyridine ligand **19** and Cu^{2+} with two bound nitrate ions (*24*). *Reproduced by permission of The RSC.*

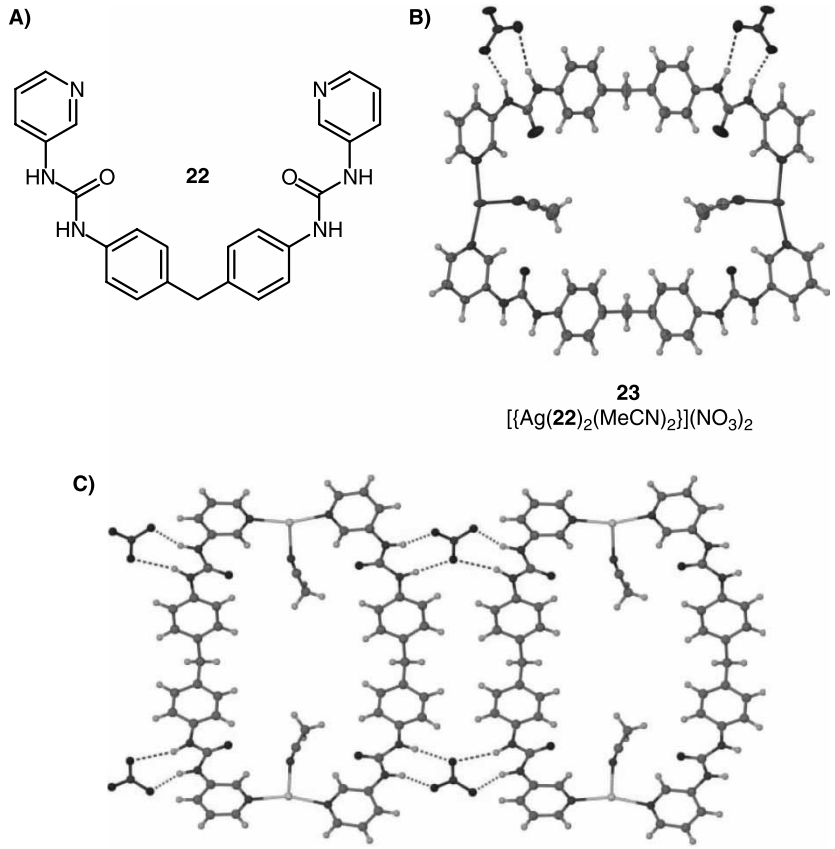

FIGURE 24 (A) ChemDraw structure of bis(ureidopyridine) ligand **22**. (B) The X-ray crystal structure of the metallomacrocycle $[\{Ag(\mathbf{22})_2(MeCN)_2\}](NO_3)_2$ aka **23**. (C) The hydrogen-bonded network between adjacent entities of **23** held together by NO_3^- ions [24,92]. *Reproduced by permission of The RSC.*

centre (Fig. 24) [24,92]. The nitrate binding properties of the bis(ureidopyridine) ligand **22** and its silver complex **23** in solution are yet to be reported.

The presence of a metal centre in these urea-based receptors (**20**–**23**) seems to enhance their affinity for NO_3^-. This may be because the orientations of the urea groups are fixed in space, enhancing the directionality and complementarity of the hydrogen bonding interactions between receptors and NO_3^-.

Guanidinium Receptors

The guanidinium moiety is frequently used in nature to coordinate anions because it can form strong ion pairs with (oxy)anions, as well as provide directional hydrogen bonding interactions. In biological systems, the guanidinium moiety is present as the side chain of the amino acid arginine and has a high pK_a value [(~12–13; *93,94*)]. This high pK_a allows the guanidinium cation to remain protonated over a wide pH range. In synthetic systems, use of the guanidinium moiety for nitrate recognition has been limited, even though it is widely used for the recognition of carboxylate and phosphate oxyanions [95].

Following Hay's recommendations that incorporating guanidinium and urea functions into the same receptor should provide ideal complementarity to an oxyanion [30], de Mendoza and co-workers [18] reported a new class of guanidine–urea receptors **24**–**27** (Scheme 8). The nitrate binding ability of receptors **24**–**27** was assessed by ^{1}H NMR and isothermal titration calorimetry (ITC) titrations in CD_3CN. Nitrate was titrated as its tetrabutylammonium salt. In NMR titrations, saturation was observed for the acyclic host **24** and the cyclic host with the shortest alkyl linker **25**, after the addition of 1.5 equivalents of nitrate. However, no accurate NMR binding data could be obtained for cyclic hosts **26** and **27** due to *in situ* crystallisation at the concentrations used for the titrations. ITC titration, which allows the determination of binding constants and thermodynamic parameters at concentrations lower than those used for NMR titration, was used to overcome this problem. ITC binding isotherms suggested formation of 1:1 host–guest complexes and the K_a values were in good agreement with ^{1}H NMR data (Table V). Binding isotherms also revealed that NO_3^- binding by receptor **25** was mainly governed by entropic factors, whereas for receptors **26** and **27**, both enthalpic and entropic factors play a significant role in NO_3^- binding. The explanation for these differences is that the cavity of macrocycle **25** is too small for optimal anion inclusion, such that

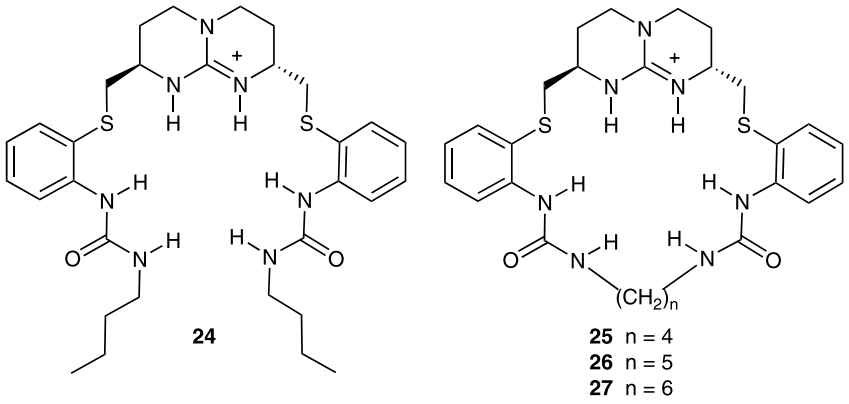

SCHEME 8 Acyclic guanidine–urea receptor **24** and its cyclic analogues **25**–**27** [18]. *Reproduced by permission of The RSC on behalf of the CNRS*.

hydrogen bonding interactions between the receptor and NO_3^- are weaker.

Solid-state evidence supports de Mendoza's hypothesis, as can be seen in the crystal structures of the nitrate complexes of macrocycles **25**–**27** (Fig. 25). The structure of the [$\mathbf{25}^+ \cdot NO_3^-$] complex is distorted, with one urea twisted away from the cavity, thus reducing the number of hydrogen bond contacts with NO_3^- to only three. In contrast, NO_3^- fits into the cavities of receptors **26** ([$\mathbf{26}^+ \cdot NO_3^-$], Fig. 25) and **27** ([$\mathbf{27}^+ \cdot NO_3^-$], Fig. 25) and makes contact with all six NH donor groups from the urea and guanidinium moieties. The crystal structures of hosts **26** and **27** also show that each oxygen atom of NO_3^- forms two hydrogen bonds with the host, such that its lone pairs are shared with single NH donors from different functions (ureas and guanidinium) in the preferred motif shown in Fig. 26 [18,34]. The nitrate complexes of macrocycles **26** and **27** are rare examples of six-coordinate NO_3^- complexes [3] and represent the ideal for NO_3^- coordination as revealed by Hay's theoretical studies [30].

The ultimate goal in the design of synthetic anion receptors is function and application such as for transmembrane transport. In this case, the ideal is a NO_3^- receptor that is capable of binding and selectively transporting the anion across bilayer membranes. Following is a discussion of one such NO_3^- receptor.

TABLE V Association constants (M^{-1}) and thermodynamic parameters for the binding of hosts **24**–**27** with tetrabutylammonium nitrate

	24	**25**	**26**	**27**
$K_a(\times 10^3)$[a]	5.50	9.94	–[c]	–[c]
$K_a(\times 10^3)$[b]	5.38	7.26	15.2	73.7
ΔH[d]	−3.73	−1.07	−3.02	−3.48
ΔS[d]	4.72	14.2	9.16	10.8
ΔG[d]	−5.16	−5.37	−5.79	−6.75

[a] Determined by ^{1}H NMR titrations in CD_3CN at 298 K; [b] Determined by ITC titrations in CH_3CN at 303 K; [c] Not determined because of *in situ* crystallisation; [d] ΔH and ΔG in kcal mol^{-1}, ΔS in cal mol^{-1} K^{-1} [18]. *Reproduced by permission of The RSC on behalf of the CNRS*.

SYNTHETIC TRANSPORTERS FOR NITRATE

Synthetic transmembrane transporters selective for nitrate are rare. A Scifinder survey yielded one result: a NO_3^- transporter developed in our laboratory [96]. To act as a transmembrane transporter, a ligand must bind the anion and move it across a phospholipid membrane. However, binding should be such that after moving the ligand across the barrier the receptor releases the ligand under appropriate conditions.

We reported a C_3-symmetric triamide NO_3^- receptor, **28**, based on the triphenoxymethane scaffold [96]. The X-ray crystal analysis of **28** revealed a structure, where three amide chains point in the same direction, creating a potential anion-binding pocket (Fig. 27).

Investigation of anion binding by **28** revealed that it coordinates Cl^- ($K_a = 816 \pm 108\,M^{-1}$) about ~2.5 times stronger than NO_3^- ($K_a = 326 \pm 113\,M^{-1}$) in CD_2Cl_2. In transmembrane transport assays, compound **28** was, however, a selective NO_3^- transporter. The anion transporting activity of **28** was compared with its *tert*-butyl analogue **29** and calixarene **30** [(97; Scheme 9)]. Transport assays were done with egg-yolk phosphatidylcholine liposomes under a pH gradient and triamide **28** transported NO_3^-, but not Cl^-, across the bilayer [96]. Assays were carried out without a pH gradient to determine the mechanism of NO_3^- transport by **28**. Nitrate-containing EYPC liposomes (pH 6.4) were suspended in a Cl^- solution (pH 6.4), treated with compounds **28**–**30** and intravesicular pH determined. As seen in Fig. 28, the addition of **28** led to an increase in the internal pH of the liposomes, whereas there was no pH change with *tert*-butyl analogue **29** or calixarene **30**. Compound **29** did not bind anions and was inactive for transmembrane Cl^- or NO_3^- transport. Differences in anion binding and transport activity between **28** and **29** were attributed to steric and electronic factors [96,97]. Compound **30**, which

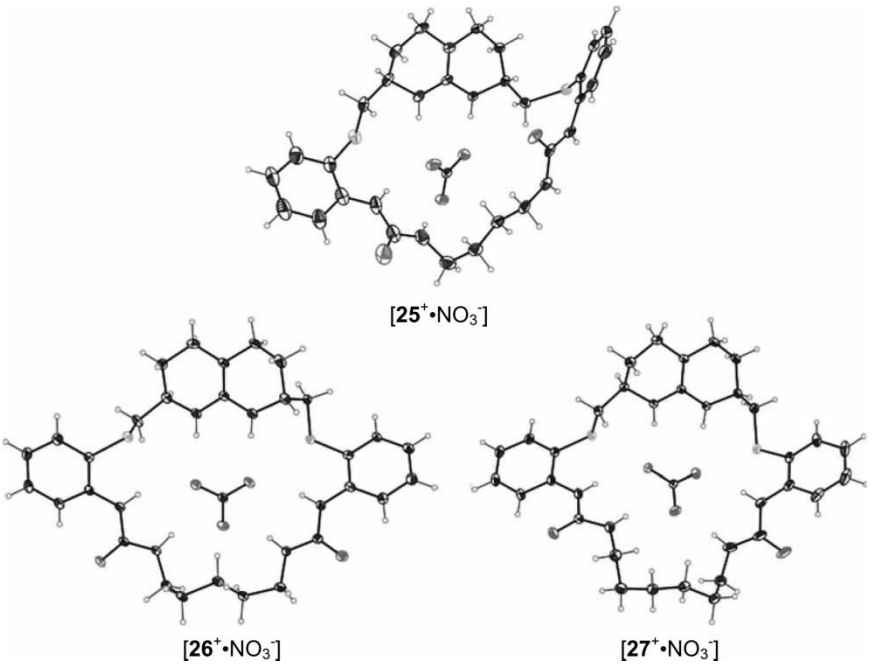

FIGURE 25 Crystal structures of the NO_3^- complexes of macrocycles **25** ([**25**$^+$·NO_3^-]), **26** ([**26**$^+$·NO_3^-]) and **27** ([**27**$^+$·NO_3^-]) [18]. *Reproduced by permission of The RSC on behalf of the CNRS.*

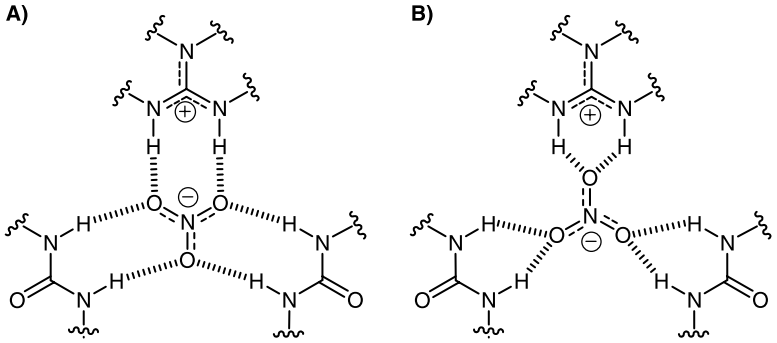

FIGURE 26 (A) The preferred six-coordinate binding motif for NO_3^- inclusion in macrocycles **25**–**27**. Each oxygen atom of NO_3^- forms hydrogen bond with one NH donor each from the urea and guanidinium functions. (B) The other possible binding motif for NO_3^- inclusion. This motif in which each oxygen atom's lone pair is hydrogen bonded to NH donors of the same function is not preferred [18]. *Reproduced by permission of The RSC on behalf of the CNRS.*

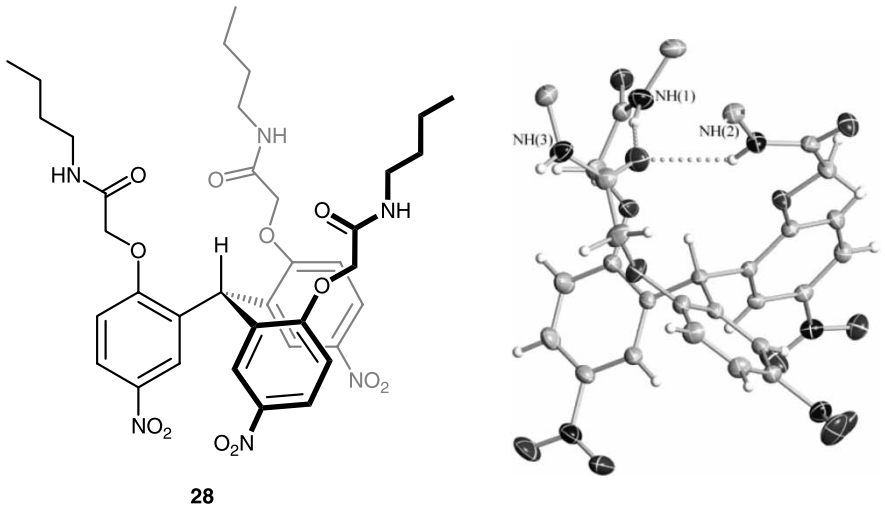

28

FIGURE 27 ChemDraw (left) and X-ray crystal (right) structure of the transmembrane NO_3^- transporter **28**. The crystal structure shows a potential anion pocket created by amide side chains: two NH groups are hydrogen bonded to the C═O group of the third chain [96]. *Reproduced by permission of The RSC.*

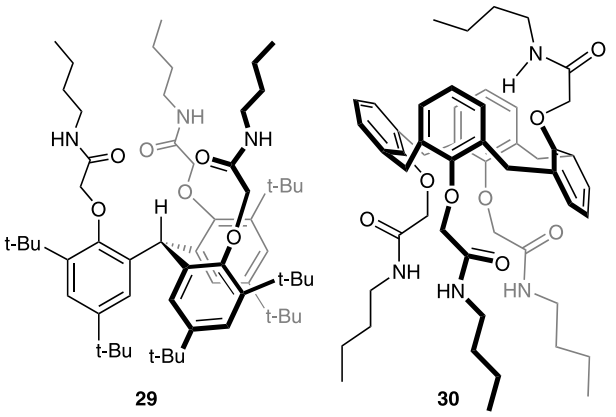

SCHEME 9 Compounds **29** and **30** compared with triamide **28** for NO_3^- binding and transport. Compound **29** is the *tert*-butyl analogue of **28** while calixarene **30** is a known transmembrane Cl^- transporter [96]. *Reproduced by permission of The RSC.*

transports Cl^- and NO_3^- [97], is a $C1^-/NO_3^-$ exchanger [96]. In contrast, triamide **28** moves NO_3^- along the $NO_3^-/C1^-$ gradient, but cannot compensate by transporting Cl^- from the extravesicular buffer into the liposome. To maintain electroneutrality, compound **28** must co-transport H^+—NO_3^- across the membrane via a H^+—NO_3^- symport (or equivalent OH^-/NO_3^- antiport) mechanism.

CONCLUSIONS

The anion recognition field has expanded greatly in the past decade [1–6]. There are, however, only a few NO_3^--selective hosts described and their selectivity is typically marginal. Nitrate binding is a weakly coordinating anion and strong hydrogen bond donors are usually needed as one component for NO_3^- anion selectivity. Additionally, charged residues within the binding site enhance association between host and guest. Shape considerations are also important for the recognition of NO_3^- in the cavities of synthetic receptors. In nature, proteins and enzymes involved in nitrate uptake and metabolism have amino residues that contribute strong hydrogen bonding and ion-pairing interactions and are arranged for maximal contacts with NO_3^-. NR utilises the Moco to bind NO_3^- anions. The presence of a metal centre in the enzyme's active site contributes to the number of effective interactions between itself and NO_3^- anions.

From the receptors discussed in this review, the difficulty of designing NO_3^--selective receptors becomes more apparent. The effective receptors combined factors such as charge, hydrogen bond directionality and shape of the cavity to select for nitrate. The identification of receptors such as the guanidine urea macrocycles **26** and **27** is a big step in the direction of rational design of nitrate-selective receptors. Even though the selectivity ratio $C1^-/NO_3^-$ of receptor **27** is moderate [(1.3; 93)], achieving a coordination number of six for NO_3^- anion (the optimal coordination number for NO_3^-) is an indication that specificity and selectivity for this anion by synthetic receptors is indeed possible.

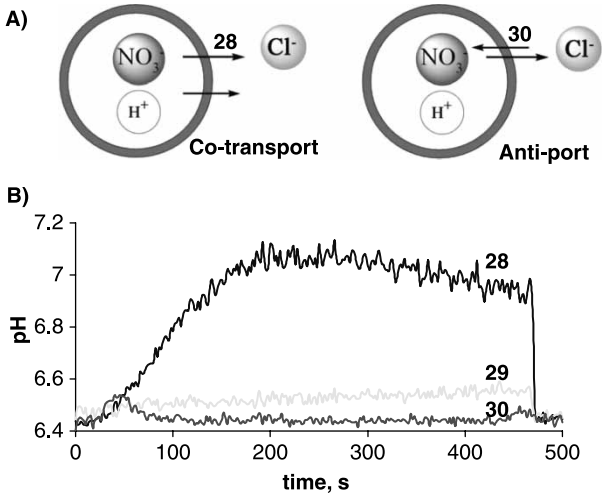

FIGURE 28 Change in extravesicular pH. (A) Triamide **28** functions as a H^+—NO_3^- co-transporter whereas calixarene **30** functions as a NO_3^-—Cl^- anion exchanger. (B) A plot of the intravesicular pH versus time in experiments where NO_3^--loaded EYPC liposomes (pH 6.4) suspended in a NaCl solution (pH 6.4) were treated with compounds **28**–**30**. Intravesicular pH was determined by monitoring the changes in the fluorescent ratios of the pH-sensitive dye, HPTS [96]. *Reproduced by permission of The RSC.*

Acknowledgements

We dedicate this paper to Professor David Reinhoudt on the occasion of his 65th birthday. We thank the Department of Energy for continued funding of our research.

References

[1] *Supramolecular Chemistry of Anions*; Bianchi, A., Bowman-James, K., García-España, E., Eds.; Wiley-VCH: New York, 1997.
[2] Sessler, J. L.; Gale, P. A.; Cho, W.-S. *Monographs in Supramolecular Chemistry: Anion Receptor Chemistry*; RSC Publishing: Cambridge, 2006.
[3] Kang, S. O.; Begum, R. A.; Bowman-James, K. *Angew. Chem. Int. Ed.* **2006**, *45*, 7882.
[4] Gale, P. A. *Acc. Chem. Res.* **2006**, *36*, 465.
[5] Beer, P. D.; Gale, P. A. *Angew. Chem. Int. Ed.* **2001**, *40*, 486.
[6] Gamez, P.; Mooibroek, T. J.; Teat, S. J.; Reedijk, J. *Acc. Chem. Res.* **2007**, *40*, 435.
[7] Lundberg, J. O.; Weitzberg, E.; Cole, J. A.; Benjamin, N. *Nat. Rev. Microbiol.* **2004**, *2*, 593.
[8] Brambilla, G.; Martelli, A. *Mutat. Res.* **2007**, *635*, 17.
[9] Mensinga, T. T.; Speijers, G. J. A.; Meulenbelt, J. *Toxicol. Rev.* **2003**, *22*, 41.
[10] Tongraar, A.; Tangkawanwanit, P.; Rode, B. M. *J. Phys. Chem. A* **2006**, *110*, 12918.
[11] Oberhammer, H. *J. Mol. Struct.* **2002**, *605*, 177.
[12] Velders, G. J. M.; Feil, D. *Theor. Chim. Acta* **1992**, *84*, 195.
[13] Hase, Y. *Monatsh. Chem.* **1985**, *116*, 1305.
[14] Love, I. *J. Phys. Chem. A* **2006**, *110*, 10507.

[15] Zhurova, E. A.; Stash, A. I.; Tsirelson, V. G.; Zhurov, V. V.; Bartashevich, E. V.; Potemkin, V. A.; Pinkerton, A. A. *J. Am. Chem. Soc.* **2006**, *128*, 14728.
[16] Ripin, D. H.; Evans, D. A.;, pKa Tableon World Wide Web URL: http://daecr1.harvard.edu/pdf/evans_pKa_table.pdf
[17] González-Lebrero, M. C.; Bikiel, D. E.; Elola, M. D.; Estrin, D. A. *J. Chem. Phys.* **2002**, *117*, 2718.
[18] Blondeau, P.; Benet-Buchholz, J.; de Mendoza, J. *New J. Chem.* **2007**, *31*, 736, http://dx.doi.org/10.1039/b616409a.
[19] Cronin, L.; McGregor, P. A.; Parsons, S.; Teat, S.; Gould, R. O.; White, V. A.; Long, N. J.; Robertson, N. *Inorg. Chem.* **2004**, *43*, 8023.
[20] Mahoney, J. M.; Stucker, K. A.; Jiang, H.; Carmichael, I.; Brinkmann, N. R.; Beatty, A. M.; Noll, B. C.; Smith, B. D. *J. Am. Chem. Soc.* **2005**, *127*, 2922.
[21] Sessler, J. L.; Camiolo, S.; Gale, P. A. *Coord. Chem. Rev.* **2003**, *240*, 17.
[22] Sessler, J. L.; Roznyatovskiy, V.; Pantos, G. D.; Borisova, N. E.; Reshetova, M. D.; Lynch, V. M.; Khrustalev, V. N.; Ustynyuk, Y. A. *Org. Lett.* **2005**, *7*, 5277.
[23] Bhattarai, K. M.; del Amo, V.; Magro, G.; Sisson, A. L.; Joos, J. B.; Charmant, J. P. H.; Kantacha, A.; Davis, A. P. *Chem. Commun.* **2006**, 2335.
[24] Steed, J. W. *Chem. Commun.* **2006**, 2637, http://dx.doi.org/10.1039/b601511e.
[25] Schazmann, B.; Diamond, D. *New J. Chem.* **2007**, *31*, 587.
[26] Kim, H.; In, S.; Kang, J. *Supramol. Chem.* **2006**, *18*, 141.
[27] Bryantsev, V. S.; Hay, B. P. *Org. Lett.* **2005**, *7*, 5031.
[28] Bryantsev, V. S.; Hay, B. P. *J. Am. Chem. Soc.* **2005**, *127*, 8282.
[29] Maheswari, P. U.; Modec, B.; Pevec, A.; Kozlevčar, B.; Massera, C.; Gamez, P.; Reedijk, J. *Inorg. Chem.* **2006**, *45*, 6637.
[30] Hay, B. P.; Gutowski, M.; Dixon, D. A.; Garza, J.; Vargas, R.; Moyer, B. A. *J. Am. Chem. Soc.* **2004**, *126*, 7925.
[31] Hay, B. P.; Dixon, D. A.; Bryan, J. C.; Moyer, B. A. *J. Am. Chem. Soc.* **2002**, *124*, 182.
[32] Jeffrey, G. A. In *An Introduction to Hydrogen Bonding*; Truhlar, D. G., Ed.; Oxford University Press: Oxford, 1997.
[33] Desiraju, G. R.; Steiner, T. *The Weak Hydrogen Bond in Structural Chemistry and Biology*; Oxford University Press: Oxford, 1999.
[34] Hay, B. P.; Firman, T. K.; Moyer, B. A. *J. Am. Chem. Soc.* **2005**, *127*, 1810.
[35] Prins, R.; de Graaff, R. A. G.; Haasnoot, J. G.; Vader, C.; Reedijk, J. *J. Chem. Soc. Chem. Commun.* **1986**, 1430.
[36] Smith, G. T.; Mallinson, P. R.; Frampton, C. S.; Farrugia, L. J.; Peacock, R. D.; Howard, J. A. K. *J. Am. Chem. Soc.* **1997**, *119*, 5028.
[37] Rosenstein, R. D.; Oberding, M.; Hyde, J. R.; Zubieta, J.; Karlin, K. D.; Seeman, N. C. *Cryst. Struct. Commun.* **1982**, *11*, 1507.
[38] Ahrens, B.; Cotton, S. A.; Feeder, N.; Noy, O. E.; Raithby, P. R.; Teat, S. J. *J. Chem. Soc. Dalton Trans.* **2002**, 2027.
[39] Mostad, A.; Natarajan, S. Z. *Kristallogr* **1985**, *172*, 175.
[40] Goodgame, D. M. L.; Newnham, S.; O'Mahoney, C. A.; Williams, D. J. *Polyhedron* **1990**, *9*, 491.
[41] Allinger, N. L.; Yuh, Y. H.; Lii, J.-H. *J. Am. Chem. Soc.* **1989**, *111*, 8551.
[42] Herges, R.; Dikmaus, A.; Jana, U.; Köhler, F.; Jones, P. G.; Dix, I.; Fricke, T.; König, B. *Eur. J. Org. Chem.* **2002**, 3004.
[43] Campbell, W. H. *Annu. Rev. Plant Physiol. Plant Mol. Biol.* **1999**, *50*, 277.
[44] Leaf, C. D.; Wishnok, J. S.; Tannenbaum, S. R. *Biochem. Biophys. Res. Commun.* **1989**, *163*, 1032.
[45] Doyle, M. P.; Hoekstra, J. W. *J. Inorg. Biochem.* **1981**, *14*, 351.
[46] Pouliquin, P.; Boyer, J.-C.; Grouzis, J.-P.; Gibra, R. *Plant Physiol.* **2000**, *122*, 265.
[47] Zhou, J.-J.; Trueman, L. J.; Boorer, K. J.; Theodoulou, F. L.; Forde, B. G.; Miller, A. J. *J. Biol. Chem.* **2000**, *275*, 39894.
[48] Moir, J. W. B.; Wood, N. J. *Cell. Mol. Life Sci.* **2001**, *58*, 215.
[49] Aichi, M.; Yoshihara, S.; Yamashita, M.; Maeda, S.-I.; Nagai, K.; Omata, T. *Biosci. Biotechnol. Biochem.* **2006**, *70*, 2682.
[50] Saier, Jr., M. H. *J. Cell. Biochem.* **1999**, *84*, S32/33.
[51] Crawford, N. M.; Glass, A. D. M. *Trends Plant Sci.* **1998**, *3*, 389.
[52] Forde, B. G. *Biochim. Biophys. Acta* **2000**, *1465*, 219.
[53] Vincill, E. D.; Szczyglowski, K.; Roberts, D. M. *Plant Physiol.* **2005**, *137*, 1435.
[54] Koropatkin, N. M.; Pakrasi, H. B.; Smith, T. J. *Proc. Natl. Acad. Sci.* **2006**, *103*, 9820.
[55] Kinghorn, J. R.; Sloan, J.; Kana'n, G. J. M.; DaSilva, E. R.; Rouch, D. A.; Unkles, S. E. *Genetics* **2005**, *169*, 1369.
[56] Unkles, S. E.; Rouch, D. A.; Wang, Y.; Siddiqi, M. Y.; Glass, A. D. M.; Kinghorn, J. R. *Proc. Natl. Acad. Sci.* **2004**, *101*, 17549.
[57] Unkles, S. E.; Rouch, D. A.; Wang, Y.; Siddiqi, M. Y.; Okamoto, M.; Stephenson, R. M.; Kinghorn, J. R.; Glass, A. D. M. *Biochemistry* **2005**, *44*, 5471.
[58] Kobayashi, M.; Rodriguez, R.; Lara, C.; Omata, T. *J. Biol. Chem.* **1997**, *272*, 27197.
[59] Kobayashi, M.; Takatani, N.; Tanigawa, M.; Omata, T. *J. Bacteriol.* **2005**, *187*, 498.
[60] Koropatkin, N. M.; Koppenaal, D. W.; Pakrasi, H. B.; Smith, T. J. *J. Biol. Chem.* **2007**, *282*, 2606.
[61] Maeda, S.; Omata, T. *J. Biol. Chem.* **1997**, *272*, 3036.
[62] Wang, Z.; Choudhary, A.; Ledvina, P. S.; Quiocho, F. A. *J. Biol. Chem.* **1994**, *269*, 25091.
[63] González, P. J.; Correia, C.; Moura, I.; Brondino, C. D.; Moura, J. J. G. *J. Inorg. Biochem.* **2006**, *100*, 1015.
[64] Hille, R. *Chem. Rev.* **1996**, *96*, 2757.
[65] Fischer, K.; Barbier, G. G.; Hecht, H.-J.; Mendel, R. R.; Campbell, W. H.; Schwarz, G. *Plant Cell* **2005**, *17*, 1167, www.plantcell.org.
[66] Jepson, B. J. N.; Mohan, S.; Clarke, T. A.; Gates, A. J.; Cole, J. A.; Butler, C. S.; Butt, J. N.; Hemmings, A. M.; Richardson, D. J. *J. Biol. Chem.* **2007**, *282*, 6425.
[67] Bertero, M. G.; Rothery, R. A.; Palak, M.; Hou, C.; Lim, D.; Blasco, F.; Weiner, J. H.; Strynadka, N. C. *J. Nat. Struct. Biol.* **2003**, *10*, 681.
[68] Brigé, A.; Leys, D.; Meyer, T. E.; Cusanovich, M. A.; van Beeumen, J. J. *Biochemistry* **2002**, *41*, 4827.
[69] Bertero, M. G.; Rothery, R. A.; Boroumand, N.; Palak, M.; Blasco, F.; Ginet, N.; Weiner, J. H.; Strynadka, N. C. J. *J. Biol. Chem.* **2005**, *280*, 14836.
[70] Arnoux, P.; Sabaty, M.; Alric, J.; Frangioni, B.; Guigliarelli, B.; Adriano, J.-M.; Pignol, D. *Nat. Struct. Biol.* **2003**, *10*, 928.
[71] Sessler, J. L.; Cho, W.-S.; Gross, D. E.; Shriver, J. A.; Lynch, V. M.; Marquez, M. *J. Org. Chem.* **2005**, *70*, 5982.
[72] Anzenbacher, Jr., P.; Try, A. C.; Miyaji, H.; Jursíková, K.; Lynch, V. M.; Marquez, M.; Sessler, J. L. *J. Am. Chem. Soc.* **2000**, *122*, 10268.
[73] Amendola, V.; Esteban-Gómez, D.; Fabbrizzi, L.; Licchelli, M. *Acc. Chem. Res.* **2006**, *39*, 343.
[74] Sessler, J. L.; An, D.; Cho, W.-S.; Lynch, V.; Marquez, M. *Chem. Eur. J.* **2005**, *11*, 2001.
[75] Bondy, C. R.; Loeb, S. J. *Coord. Chem. Rev.* **2003**, *240*, 77.
[76] Kang, Md., S. O.; Hossain, A.; Bowman-James, K. *Coord. Chem. Rev.* **2006**, *250*, 3038.
[77] Bisson, A. P.; Lynch, V. M.; Monahan, M.-K. C.; Anslyn, E. V. *Angew. Chem. Int. Ed. Engl.* **1997**, *36*, 2340.
[78] Niikura, K.; Bisson, A. P.; Anslyn, E. V. *J. Chem. Soc. Perkin Trans.* **1999**, *2*, 1111.
[79] Deetz, M. J.; Shang, M.; Smith, B. D. *J. Am. Chem. Soc.* **2000**, *122*, 6201.
[80] Mahoney, J. M.; Davis, J. P.; Beatty, A. M.; Smith, B. D. *J. Org. Chem.* **2003**, *68*, 9819.
[81] Mahoney, J. M.; Nawaratna, G. U.; Beatty, A. M.; Duggan, P. J.; Smith, B. D. *Inorg. Chem.* **2004**, *43*, 5902.
[82] Choi, K.; Hamilton, A. D. *J. Am. Chem. Soc.* **2003**, *125*, 10241.
[83] García-España, E.; Díaz, P.; Llinares, J. M.; Bianchi, A. *Coord. Chem. Rev.* **2006**, *250*, 2952.
[84] Llinares, J. M.; Powell, D.; Bowman-James, K. *Coord. Chem. Rev.* **2003**, *240*, 57.
[85] Papoyan, G.; Gu, K.-J.; Wiórkiewicz-Kuczera, J.; Kuczera, K.; Bowman-James, K. *J. Am. Chem. Soc.* **1996**, *118*, 1354.
[86] Wiórkiewicz-Kuczera, J.; Kuczera, K.; Bazzicalupi, C.; Bencini, A.; Valtancoli, B.; Bianchi, A.; Bowman-James, K. *New. J. Chem.* **1999**, *23*, 1007.
[87] Mason, S.; Clifford, T.; Seib, L.; Kuczera, K.; Bowman-James, K. *J. Am. Chem. Soc.* **1998**, *120*, 8899.
[88] Schneider, J. P.; Pochan, D. J.; Ozbas, B.; Rajagopal, K.; Pakstis, L.; Kretsinger, J. *J. Am. Chem. Soc.* **2002**, *124*, 15030.
[89] Hynes, M. J.; Maubert, B.; McKee, V.; Town, R. M.; Nelson, J. *J. Chem. Soc. Dalton Trans.* **2000**, 2853, http://dx.doi.org/10.1039/b003249m.

[90] Turner, D. R.; Smith, B.; Spencer, E. C.; Goeta, A. E.; Radosavljevic-Evans, I.; Tocher, D. A.; Howard, J. A. K.; Steed, J. W. *New J. Chem.* **2005**, *29*, 90, http://dx.doi.org/10.1039/b415818k.
[91] Russell, J. M.; Parker, A. D. M.; Radosavljevic-Evans, I.; Howard, J. A. K.; Steed, J. W. *Chem. Commun.* **2006**, 269.
[92] Applegarth, L.; Clark, N.; Richardson, A. C.; Parker, A. D. M.; Radosavljevic-Evans, I.; Goeta, A. E.; Howard, J. A. K.; Steed, J. W. *Chem. Commun.* **2005**, 5423, http://dx.doi.org/10.1039/b511259a.
[93] Blondeau, P.; Segura, M.; Pérez-Fernández, R.; de Mendoza, J. *Chem. Soc. Rev.* **2007**, *36*, 198.
[94] Schug, K. A.; Lindner, W. *Chem. Rev.* **2005**, *105*, 67.
[95] Houk, R. J. T.; Tobey, S. L.; Anslyn, E. V. *Top. Curr. Chem.* **2005**, *255*, 199.
[96] Santacroce, P. V.; Okunola, O. A.; Zavalij, P. Y.; Davis, J. T. *Chem. Commun.* **2006**, 3246, http://dx.doi.org/10.1039/b607221f.
[97] Seganish, J. L.; Santacroce, P. V.; Salimian, K. L.; Fettinger, J. C.; Zavalij, P.; Davis, J. T. *Angew. Chem. Int. Ed.* **2006**, *45*, 3334.